General Disclaimer

One or more of the Following Statements may affect this Document

- This document has been reproduced from the best copy furnished by the organizational source. It is being released in the interest of making available as much information as possible.

- This document may contain data, which exceeds the sheet parameters. It was furnished in this condition by the organizational source and is the best copy available.

- This document may contain tone-on-tone or color graphs, charts and/or pictures, which have been reproduced in black and white.

- This document is paginated as submitted by the original source.

- Portions of this document are not fully legible due to the historical nature of some of the material. However, it is the best reproduction available from the original submission.

UNIVERSITY OF ILLINOIS
URBANA

AERONOMY REPORT NO. 73

ANALYSIS OF SOUNDING ROCKET DATA FROM PUNTA CHILCA, PERU

by
R. W. Fillinger, Jr.
E. A. Mechtly
E. K. Walton

July 1, 1976

Library of Congress ISSN 0568-0581

Aeronomy Laboratory
Department of Electrical Engineering
University of Illinois
Urbana, Illinois

Supported by
National Aeronautics and Space Administration
Grant NGR 14-005-181

UILU-ENG 76 2504

A E R O N O M Y R E P O R T

N O. 73

ANALYSIS OF SOUNDING ROCKET DATA FROM PUNTA CHILCA, PERU

by

R. W. Fillinger, Jr.
E. A. Mechtly
E. K. Walton

July 1, 1976

Supported by
National Aeronautics
and Space Administration
Grant NGR 14-005-181

Aeronomy Laboratory
Department of Electrical Engineering
University of Illinois
Urbana, Illinois

ABSTRACT

The United States National Aeronautics and Space Administration in cooperation with 12 scientific groups launched 26 sounding rockets from the equatorial launch site at Punta Chilca, Peru during the period May 20, 1975 to June 10, 1975. The purpose of this cooperative effort is to study in detail the structure and dynamics of the equatorial atmosphere between 20 and 160 km altitude. Three of the 26 rocket payloads were built by the Aeronomy Laboratory of the Department of Electrical Engineering of the University of Illinois at Urbana-Champaign. These payloads were designed to investigate the anomalous properties of the equatorial ionosphere. The objectives of the UI payloads included

1. A measure of electron temperature,
2. A measure of electron concentration in the lower ionosphere,
3. An observation of the fine structure in the profile of electron concentration, and
4. An examination of the role of energetic electrons as a nighttime source of ionization.

This report discusses in detail a technique for measuring electron concentrations in the lower portion of the ionosphere above Punta Chilca. The technique combines a radio-propagation experiment for measuring Faraday rotation and a dc/Langmuir probe experiment for measuring electron current. The results obtained from the analysis of radio and probe data from Nike Apache 14.532, which was launched at 20:26 UT on May 28, 1975, at a solar zenith angle of 60°, are presented in Chapter 5. A comparison of the profiles of electron concentration, N, from Nike Apache 14.532 and *Kane* [1974] indicates that the value of the maximum ionization in the D region, $N_m D$, under quiet conditions is proportional to the square of the cosine of the solar zenith angle.

TABLE OF CONTENTS

LIST OF FIGURES

LIST OF TABLES

1. INTRODUCTION

Twenty-six sounding rockets were launched during the period May 20 to June 10, 1975 by the United States National Aeronautics and Space Administration in cooperation with 12 scientific groups to study in detail the structure and dynamics of the equatorial atmosphere between 20 and 160 km altitude. The rockets were launched from Punta Chilca, Peru, at the geomagnetic equator.

The Aeronomy Laboratory of the Department of Electrical Engineering of the University of Illinois at Urbana-Champaign built three of the 26 rocket payloads. The payloads were designed to investigate the anomalous properties of the equatorial ionosphere. More specifically, the objectives of the UI payloads included

1. A comparison of electron temperatures measured by three techniques:
   (a) The University of Illinois Langmuir probe
   (b) An RF resonance probe supplied by Dr. K. Hirao and Dr. K. Oyama of the University of Tokyo
   (c) The incoherent-scatter radar at Jicamarca, Peru
2. A measure of the electron concentration in the lower ionosphere;
3. An observation of the fine structure in the profile of electron concentration to examine the role of vertical transport in layering metallic ions; and
4. An examination of the role of energetic electrons as a nighttime source of ionization.

This thesis discusses the technique used for measuring the electron concentrations in the lower portion of the ionosphere above Punta Chilca. The technique combines a radio-propagation experiment for measuring Faraday rotation and a Langmuir dc-probe experiment for measuring electron current.

Although the probe cannot measure electron concentration directly, its high-resolution measurements of changes in electron concentration are calibrated by the radio-propagation experiment which accurately measures electron concentration but with poor altitude resolution.

A brief discussion of the Appleton-Hartree and Sen-Wyller theories is presented in Chapter 2. Chapter 3 describes the operating principles of the radio-propagation and dc-probe experiments. A method of processing the radio-propagation data to obtain Faraday rotation (differential phase) rates and a method, based on the generalized magnetoionic theory for analyzing the Faraday rotation rates is presented in Chapter 4. These methods are applied to radio and probe data from Nike Apache 14.532, which was launched at 20:26 UT on May 28, 1975, at a solar zenith angle of 60°. The data from the two nighttime shots, Nike Apaches 14.524 and 14.525, are still being analyzed and will not be presented here.

2. MAGNETOIONIC THEORY

The equations of magnetoionic theory describe the propagation of radio waves through ionized media, upon which is superposed an external magnetic field. The ionosphere and magnetic field of the earth constitute a magnetoionic medium. In upper regions of the ionosphere, collisions of electrons are negligible, and magnetoionic theory reduces to its simpler form, the Appleton-Hartree equations [*Appleton*, 1932; *Hartree*, 1931] which are useful for discussion of wave polarization. In the lower region of the ionosphere, collisions are important. They result in the conversion of electromagnetic energy from the radio waves to heat. In this region a more generalized theory is necessary. Generalized magnetoionic theory is expressed by the Sen-Wyller equations [*Sen and Wyller*, 1960] which must be used in discussions of radio-wave absorption. The Sen-Wyller equations are used in Chapter 4 for the analysis of radio-propagation data.

2.1 *Appleton-Hartree Theory*

An important property of wave propagation in an anisotropic medium, such as the earth's ionosphere, is the occurrence of normal modes or characteristic waves. A characteristic wave is a wave which propagates in a given uniform medium without changing its wave polarization. In an anisotropic medium there exist two characteristic waves, each having a distinct polarization and refractive index. The theory of Appleton-Hartree describes the polarizations and the refractive indices of these modes in the ionosphere under the following assumptions: electron collisions with neutrals are independent of electron energies, the medium is electrically neutral with a uniform charge distribution, the magnetic field is uniform throughout the medium and the wave frequency is much larger than all ionic gyrofrequencies. When the wave frequency is much larger than all the ionic gyrofrequencies,

induced ionic motions are negligible because of the relatively large mass of the ions. Thus, the ions form a stationary neutralizing background.

Maxwell's curl equations for plane waves of the form

$$\vec{E} = \vec{E}_o \exp\ [j(\omega t - \vec{k}z)] \tag{2.1}$$

are

$$\vec{D} = (-n/c)\hat{z} \times \vec{H} \tag{2.2}$$

$$\vec{H} = (\varepsilon_o/\mu_o)^{\frac{1}{2}}\ n\hat{z} \times \vec{E} \tag{2.3}$$

where

$k \equiv$ wave number (rad m^{-1})

$\omega \equiv$ wave frequency (Hz)

$n \equiv$ index of refraction

$c \equiv$ velocity of light (m/s)

$\varepsilon_o \equiv$ permittivity of free space (F/m)

$\mu_o \equiv$ permeability of free space (H/m)

$\vec{H} \equiv$ magnetic field intensity (A/m)

$\vec{D} \equiv$ electric flux density (C/m)

$\vec{E} \equiv$ electric field intensity (V/m)

and

$$\vec{E}_o = E_x\hat{x} + E_y\hat{y} \tag{2.4}$$

The wave polarization ρ is defined [*Budden*, 1961] as

$$\rho \equiv -\frac{H_x}{H_y} = \frac{E_y}{E_x} = \frac{P_y}{P_x} \tag{2.5}$$

where

P_x and P_y are the polarization densities (C/m^2) in the x and y directions. The indices of refraction for fields in the form of equation (2.4) are given by

$$n^2 = 1 + \frac{P_x}{\varepsilon_o E_x} = 1 + \frac{P_y}{\varepsilon_o E_y} = \frac{k}{\omega\sqrt{\varepsilon_o\mu_o}} \tag{2.6}$$

The electric field intensity is related to the polarization density by:

$$\varepsilon_o E = \overline{\overline{\psi}}^{-1} \cdot \vec{P} \tag{2.7}$$

where the inverse of the susceptibility tensor is

$$\overline{\overline{\psi}}^{-1} = \frac{-1}{X} \begin{pmatrix} 1 & -jY_L & jY_T \\ jY_L & 1 & 0 \\ -jY_T & 0 & 1 \end{pmatrix} \tag{2.8}$$

for regions in which collisions may be neglected, and

$$X = \frac{\omega_N^2}{\omega^2} = \frac{Ne^2}{\varepsilon_o m} \cdot \frac{1}{\omega^2}$$

$$Y_L = \frac{-eB}{m} \cos \phi$$

$$Y_T = \frac{-eB}{m} \sin \phi$$

$\omega_N \equiv$ plasma frequency (rad/s)

$e \equiv$ magnitude of electronic charge (C)

$m \equiv$ electron mass (kg)

$N \equiv$ electron concentration (m^{-3})

$B \equiv$ magnitude of the magnetic flux density, $\vec{B}$ (Wb/m^2)

$\phi \equiv$ angle between the wave normal and $\vec{B}$

Combining equation (2.7) with Maxwell's equations (2.2) and (2.3) results in the following quadratic equation in ρ

$$\rho^2 - j\frac{Y_T^2/Y_L}{1-X}\rho + 1 = 0 \tag{2.9}$$

Applying the quadratic formula to (2.9) yields the following roots:

$$\rho = j \frac{Y_T^2/2Y_L}{1-X} \mp \left(\frac{1+Y_T^4/4Y_L^2}{1+X}\right)^{\frac{1}{2}} \tag{2.10}$$

The solution for the square of the refractive index is

$$n^2 = 1 - \frac{X}{1+jY_L\rho} \tag{2.11}$$

Equations (2.10) and (2.11) are known as the Appleton-Hartree equations (collisionless case).

For rocket flights from Punta Chilca, Peru (Geog. Lat. 12° 30' S, Geog. Long. 76° 48' W) the direction of the propagated radio wave is approximately transverse to the earth's magnetic field. In this case, the quasi-transverse approximation of the Appleton-Hartree equations is valid.

$$Y_T^2/4Y_L^2 >> |(1-X)^2| \tag{2.12}$$

Applying this approximation to equations (2.10) and (2.11) yields the following results:

$$\rho_o = 0 \tag{2.13a}$$

$$n_o^2 = 1 - X \tag{2.13b}$$

$$\rho_x = \infty \tag{2.14a}$$

$$n_x^2 = 1 - \frac{X}{1-X-Y_T^2} \tag{2.14b}$$

where the subscripts o and x refer to the ordinary and extraordinary waves, respectively. Equation (2.13a) shows that the ordinary wave is linearly polarized with its electric vector parallel to the earth's magnetic field, while equation (2.14a) shows that the extraordinary wave is linearly polarized with its electric vector perpendicular to the earth's magnetic field.

2.2 *The Sen-Wyller Theory*

In the region of the lower ionosphere between about 50 and 90 km, the collisions of electrons with neutral molecules appreciably influence the refractive and absorption indices of radio waves which are suitable for investigating this region. The proportionality of electron collision frequency and electron kinetic energy established by *Phelps and Pack* [1959] is an essential part of the equations for the numerical analysis of experimental data. The generalized magnetoionic theory which takes into account the

proportionality of electron collision frequency and electron kinetic energy was developed by *Sen and Wyller* [1960].

Sen and Wyller expresed the refractive index and wave polarization as functions of the elements of the permittivity tensor, $\overline{\overline{\varepsilon}}$.

$$n = \frac{(A+B\sin^2\phi \pm (B^2\sec^{-4}\phi - C^2\cos^2\phi)^{\frac{1}{2}})^{\frac{1}{2}}}{D + E\sin^2\phi} \tag{2.15}$$

$$\rho = -[B\sin^2\phi \mp (B^2\sin^4\phi - C^2\cos^2\phi)^{\frac{1}{2}}]/C\cos\phi \tag{2.16}$$

where

$$\begin{aligned} A &= 2\varepsilon_I(\varepsilon_I + \varepsilon_{III}) \\ B &= \varepsilon_{III}(\varepsilon_I + \varepsilon_{III}) + \varepsilon_{II}^2 \\ C &= 2\varepsilon_I\varepsilon_{II} \\ D &= 2\varepsilon_I \\ E &= 2\varepsilon_{III} \end{aligned} \tag{2.17}$$

The elements of the diagonalized permittivity tensor are

$$\begin{aligned} \varepsilon_I &= (1-a) - jb \\ \varepsilon_{II} &= (1/2)(f-d) + (j/2)(c-e) \\ \varepsilon_{III} &= [a-(1/2)(c+e)] + j[b-(1/2)(f+d)] \end{aligned} \tag{2.18}$$

where

$$\begin{aligned} a &= (\omega_p^2/\nu_m^2)\ C_{3/2}(\omega/\nu_m) \\ b &= (5\omega_p^2/2\omega\nu_m)\ C_{5/2}(\omega/\nu_m) \\ c &= [\omega_p^2(\omega-\omega_H)/\omega\nu_m^2]\ C_{3/2}(\omega-\omega_H)/\nu_m \\ d &= (5\omega_p^2/2\omega\nu_m)\ C_{5/2}(\omega-\omega_H)/\nu_m \\ e &= [\omega_p^2(\omega+\omega_H)/\omega\nu_m^2]\ C_{3/2}(\omega+\omega_H)/\nu_m \\ f &= (5\omega_p^2/2\omega\nu_m)\ C_{5/2}(\omega+\omega_H)/\nu_m \end{aligned} \tag{2.19}$$

and ν_m is the collision frequency associated with the most probable electron energy, assuming a Maxwell-Boltzmann distribution of electron energies. The

semi-conductor integrals are

$$C_p(x) \equiv (1/p!) \int_0^\infty \frac{u^p \, e^{-u}}{u^2+x^2} \, du \tag{2.20}$$

Although the Sen-Wyller equations provide the necessary tool for determining the electron concentration, an explicit solution for N is not available because of the great complexity of these equations. In practice, electron concentrations are calculated from differential absorption and Faraday rotation rates by an iterative computer algorithm [*Mechtly et al.*, 1970] which is based on the Sen-Wyller equations, (2.12) through (2.17).

3. RADIO PROPAGATION AT THE MAGNETIC EQUATOR

The feasibility of measuring the small differential absorption and differential phase rates anticipated at Punta Chilca are discussed in Sections 3.1 and 3.2. The rates near the geomagnetic equator are only 0.1 to 0.01 times those typically observed at midlatitudes.

3.1 *Differential Absorption at the Magnetic Equator*

To ascertain whether or not differential absorption measurements are feasible at the geomagnetic equator, radio-wave absorptions anticipated at Punta Chilca were calculated by the FORTRAN program ANALYSIS of DA, without FR, given CF model and the subroutines COEF, FIELD and SENYWL [*Mechtly et al.*, 1970]. A model profile of electron concentration, shown in Figure 3.1, was constructed from a composite of the profiles of the Croatan series, 14.228, 14.230 and 14.232 [*Mechtly et al.*, 1969]. All of these profiles are daytime profiles, χ (solar zenith angle) $\sim 60°$. Electron concentrations at particular altitudes were found by graphical interpolation. Corresponding collision frequencies were obtained from the equation

$$\nu_m = K \cdot p \quad , \tag{3.1}$$

where K equals 7.5×10^5 $N^{-1}m^2s^{-1}$ and p is the neutral atmospheric pressure (Nm^{-2}) taken from the COSPAR International Reference Atmosphere Model [*CIRA*, 1965]. For this particular situation, ν_m was calculated at 5 km intervals, from 50 to 100 km. Rocket altitudes and velocities were selected from the trajectory of Nike Apache 14.440. Calculated single mode absorptions and differential absorptions are given in Table 3.1.

Knoebel et al. [1966] estimated that the maximum resolution for differential absorption measurements is approximately ± 0.20 dB s^{-1}, or ± .133 dB km^{-1}, assuming a rocket velocity of 1500 ms^{-1}. Similar estimates were reported by *Mechtly* [1974], and *Ginther and Smith* [1975]. A direct

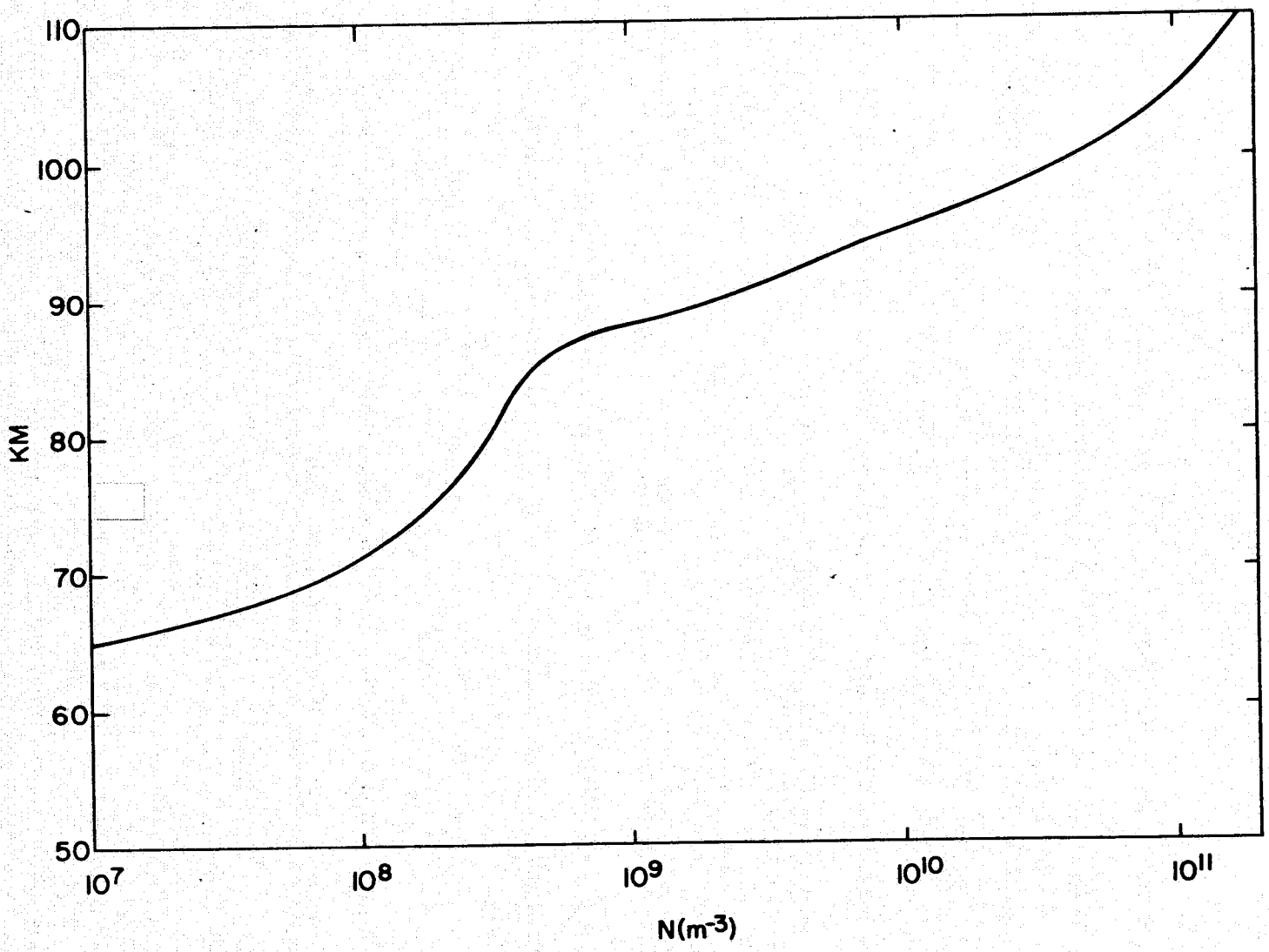

Figure 3.1 Composite electron concentration profile of Croatan shots 14.228-14.232.

TABLE 3.1

Anticipated single-mode absorptions and differential absorptions.

Frequency = 2.114 MHz

ALTITUDE (km)	O-MODE Absorption (dB/km)	X-MODE Absorption (dB/km)	DA (dB/km)
65	.014	.014	.0007
70	.112	.128	.016
75	.173	.220	.046
80	.120	.171	.051
85	.088	.128	.040
90	.149	.220	.071
95	.375	.623	.248
100	Reflection level		

Frequency = 3.145 MHz

65	.010	.010	.0004
70	.065	.071	.0059
75	.088	.100	.012
80	.055	.065	.010
85	.040	.047	.007
90	.067	.079	.012
95	.160	.193	.033
100	.406	.577	.171

comparison between the estimates of system resolution and the anticipated results of Table 3.1 shows that the sensitivity of the experiment is too low to measure differential absorption at the geomagnetic equator for solar zenith angles of 60° or larger.

3.2 *Differential Phase or Faraday Rotation*

At middle latitudes, the two circularly polarized characteristic waves are radiated from the ground at different amplitudes. They combine to form an elliptically polarized wave whose axis rotates as the wave propagates through the ionosphere because of the changing relative phase of the two component characteristic waves. An analogous situation occurs at equatorial latitudes. At the geomagnetic equator, the characteristic waves are linearly polarized and mutually perpendicular. When these characteristic waves combine, a resultant wave is produced whose polarization varies with the relative phase of the two characteristic waves. Whenever the two characteristic waves are in phase or 180° out of phase the resultant wave will be linearly polarized. However, when the characteristic waves are out of phase the resultant wave is elliptically polarized. The variations, caused by the ionosphere, of the polarization of the resultant wave is analogous to Faraday rotation at middle latitudes. An illustration of the concept of Faraday rotation at the geomagnetic equator is presented in Figure 3.2.

P. E. Monro [*Edwards*, 1974] expressed the field vectors for the linearly polarized ordinary and extraordinary waves at the magnetic equator, and derived equations for the rocket receiver output signal, W, as follows:

$$\vec{S}_o = \hat{x}\, A \sin\{(\omega-\omega_R/2)t - k_o z\} - \hat{y}\rho A \cos\{(\omega-\omega_R/2)t - k_o z\} \qquad (3.2)$$

and

$$\vec{S}_x = \hat{x}\,\rho R A \sin\{(\omega+\omega_R/2) - k_x z\} + \hat{y}\, R\, A \cos\{(\omega+\omega_R/2)\, t - k_x z\} \qquad (3.3)$$

where

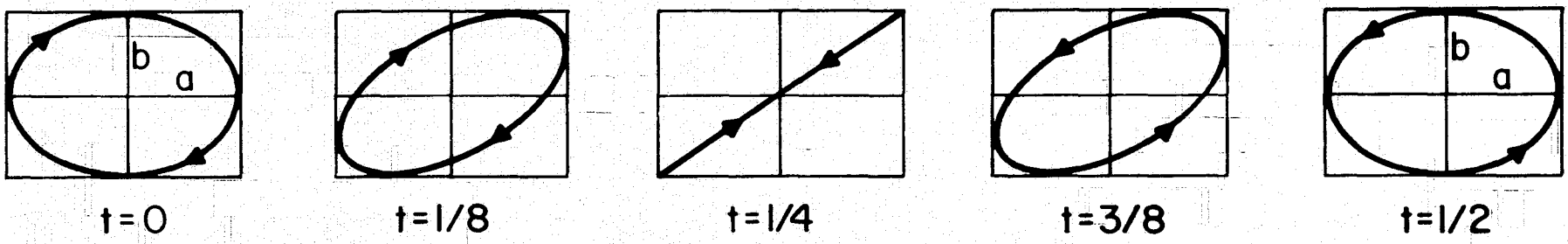

Figure 3.2. Illustration on the concept of Faraday rotation at the equator [*Rao*, 1967].

$\omega = 2\pi f \equiv$ propagation frequency (rad s^{-1})

$\omega_R = 2\pi f_R \equiv$ frequency differential between the ordinary and extraordinary wave, often referred to as the reference frequency (rad s^{-1})

$k_o, k_x \equiv$ wave numbers for the ordinary and extraordinary waves (rad m^{-1})

$R \equiv$ ratio of the ordinary wave amplitude to the extraordinary wave amplitude

$A \equiv$ constant

$\hat{x}$, $\hat{y} \equiv$ unit vectors in the x and y directions, respectively

$\rho \equiv$ wave polarization

The receiving antenna in the rocket payload is perpendicular to the rocket axis. Thus, the unit vector $\hat{\imath}$ in the direction of the antenna is given by

$$\hat{\imath} = -\hat{x} \sin \omega_s t + \hat{y} \cos \omega_s t \tag{3.4}$$

where $\omega_s = 2\pi f_s \equiv$ rocket spin rate (rad s^{-1})

The signal at the output of the antenna is proportional to the scalar product of (3.4) with the sum of (3.2) and (3.3). Substituting $z = v_R t$ for the z coordinate of the antenna into this product yields:

$$V = -\sin(\omega-\omega_R/2-k_o v_R)t \sin \omega_s t - R \sin(\omega+\omega_R/2-k_x v_R)t \sin \omega_s t + R \cos(\omega+\omega_R/2-k_x v_R)t \cos \omega_s t - \rho \cos(\omega-\omega_R-k_o v_R)t \cos \omega_s t \tag{3.5}$$

where v_R is the rocket speed (m/s). Applying the trigonometric identifies for the cosine of the sum and difference of two angles to equation (3.5) one obtains

$$V = \frac{1-\rho}{2} \cos(\omega-\omega_R/2-k_o v_R+\omega_s)t - \frac{1+\rho}{2} \cos(\omega-\omega_R/2-k_o v_R-\omega_s)t + \frac{R}{2}(1-\rho) \cos(\omega+\omega_R/2-k_x v_R-\omega_s)t + \frac{R}{2}(1+\rho) \cos(\omega+\omega_R/2-k_x v_R+\omega_s)t \tag{3.6}$$

Equation (3.6) represents the amplitude-modulated signal detected in the receiver. The output of the receiver is simply the modulation signal which can be extracted from the above equation by converting it to complex exponential form and factoring out exp ($j\omega t$). The modulus of the resultant expression is the receiver output W which becomes

$$W = \left[\frac{1+R^2}{2}(1+\rho^2) + \frac{R^2-1}{2}(1-\rho^2)\cos 2\omega_s t \right.$$
$$+ \frac{R}{2}(1-\rho)^2 \cos\{\omega_R + (k_o-k_x)v_R - 2\omega_s\}t \qquad (3.7)$$
$$\left. - \frac{R}{2}(1+\rho)^2 \cos\{\omega_R + (k_o-k_x)v_R + 2\omega_s\}t\right]^{1/2}$$

A second-order binomial expansion and normalization to reduce the dc term of this expression to unity yields

$$W = 1 + D\cos 2\omega_s t + E\cos\{\omega_R+\omega_F-2\omega_s\}t$$
$$+ F\cos\{\omega_R+\omega_F+2\omega_s\}t - 1/2\ DE\cos\{\omega_R+\omega_F-4\omega_s\}t \qquad (3.8)$$
$$+ (DE+DF)\cos\{\omega_R+\omega_F\}t + DF\cos\{\omega_R+\omega_F+4\omega_s\}t$$

where

$$\omega_F = 2\pi f_F = (k_o-k_x)v_R$$
$$D = \frac{(R^2-1)(1-\rho^2)}{2(1+R^2)(1+\rho^2)}$$
$$E = \frac{R(1-\rho)^2}{2(1+R^2)(1+\rho^2)} \qquad (3.9)$$
$$F = \frac{-R(1+\rho)^2}{2(1+R^2)(1+\rho^2)}$$

Since the characteristic waves are linearly polarized at the geomagnetic equator, we set ρ equal to zero or infinity.

The principal components of the receiver output signal containing the Faraday rotation rate, ω_F, are

$$E \cos \omega_2 t \tag{3.10}$$

$$F \cos \omega_4 t \tag{3.11}$$

$$-1/2\ DE \cos \omega_1 t \tag{3.12}$$

$$(DE+DF) \cos \omega_3 t \tag{3.13}$$

$$DF \cos \omega_5 t \tag{3.14}$$

where

$$\begin{aligned} f_1 &= \omega_1/2\pi \equiv f_R + f_F - 4f_s \\ f_2 &= \omega_2/2\pi \equiv f_R + f_F - 2f_s \\ f_3 &= \omega_3/2\pi \equiv f_R + f_F \\ f_4 &= \omega_4/2\pi \equiv f_R + f_F + 2f_s \\ f_5 &= \omega_5/2\pi \equiv f_R + f_F + 4f_s \end{aligned} \tag{3.15}$$

Examination of equation (3.8) for the receiver output reveals that the components given in equations (3.10) and (3.11) are dominant. Differentiating both (3.10) and (3.11) with respect to R and setting the derivatives equal to zero enables us to obtain conditions on R such that amplitudes of terms containing ω_F will be extrema.

$$\frac{dE}{dR} = 1/2\ \frac{(1+R^2)-2R^2}{(1+R^2)^2} = 0 \tag{3.16}$$

$$\frac{1-R^2}{2(1+R^2)^2} = 0 \tag{3.17}$$

$$1-R^2 = 0 \tag{3.18}$$

$$R = 1 \tag{3.19}$$

Similarly,

$$\frac{dF}{dR} = 1/2\ -\ \frac{(1+R^2)+2R^2}{(1+R^2)^2} \tag{3.20}$$

$$\frac{R^2-1}{(1+R^2)^2} = 0 \tag{3.21}$$

$$R^2-1 = 0 \tag{3.22}$$

$$R = 1 \tag{3.23}$$

By substituting values greater than or less than 1 for R into the expression for E and F one can easily verify that $R = 1$ maximizes E and F. That is, the Faraday amplitudes are maximized if equal ordinary and extraordinary wave amplitudes are transmitted.

3.3 *System Modifications for the Equatorial Radio-Propagation Experiment*

Instrumentation for the propagation experiment at midlatitudes is described by *Knoebel et al.* [1965].

With results of Sections 3.1 and 3.2 in mind, the following modifications were adopted for the equatorial propagation experiment at Punta Chilca, Peru:

1. Linearly polarized modes of equal amplitudes were transmitted.
2. The aspect magnetometer sensor and the rocket receiving antenna were aligned parallel to each other.
3. The differential absorption experiment was excluded.

A system using linearly-polarized antennas for transmission and reception, and a frequency differential of 500 Hz between the ordinary and extraordinary waves would produce an output at the rocket receiver as shown in Figure 3.3. An idealized situation in which the rocket velocity vector and the wave normals are in the same direction, and which neglects any nonlinearities in the rocket-borne receiver is assumed. The axis of the aspect magnetometer is aligned with the ferrite rod antenna inside the rocket for this example, and in the case of payload hardware, to simplify data interpretation. Thus, the ordinary wave is sampled during the zero-crossings of the magnetometer output, while the extraordinary wave is sampled when the magnetometer output is a maximum or minimum as demonstrated in Figure 3.3.

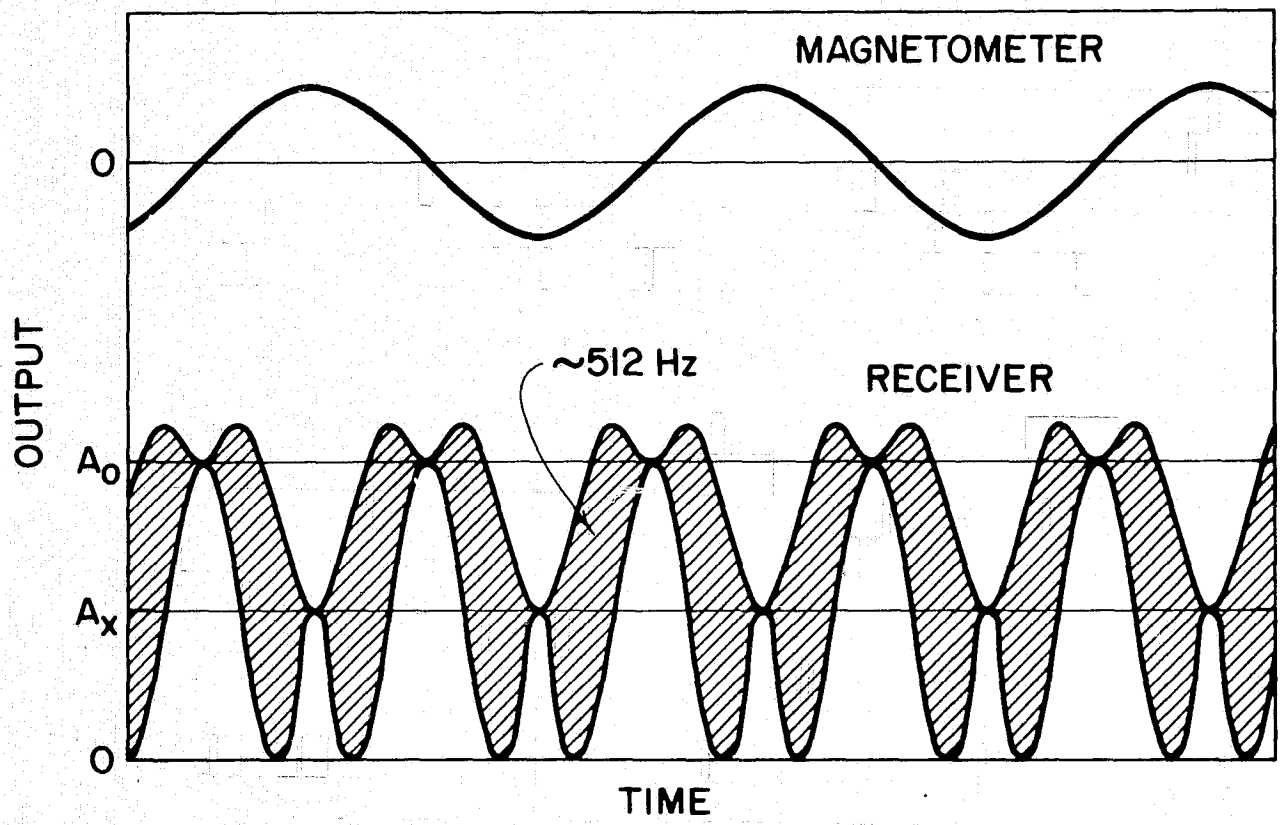

Figure 3.3. Rocket receiver output and the corresponding magnetometer output [P. E. Monro, in *Edwards*, 1974].

In each payload, the aspect magnetometer sensor was aligned with the 2.114 MHz receiving antenna.

Two crystal controlled oscillators, separated by f_R (nominally 500 Hz), generate the ordinary and extraordinary wave frequencies. The frequencies of the ordinary and extraordinary are given by $f_o = f_c$ - 250 Hz and $f_x = f_c$ + 250 Hz, respectively. f_c is the center frequency chosen for a given rocket shot. In the case of Nike Apache 14.532, the center frequencies for the radio-wave propagation experiments were 3.145 MHz and 2.114 MHz. Each mode is transmitted to the antenna dipoles by two 1-kW transmitters. The frequency, amplitude, and phase of the voltages applied to the dipoles are controlled so that both magnetoionic modes are radiated vertically. A block diagram of the system is shown in Figure 3.4.

The transmitting antenna arrays, shown in Figure 3.5, consist of two half-wavelength dipoles arranged at right angles to each other. The dipole radiating the ordinary mode was aligned parallel to the magnetic field, while the dipole radiating the extraordinary mode was aligned perpendicular to the magnetic field. The dipoles for each array were supported by three vertical wooden poles, one pole at each vertex of an isoceles right triangle. The poles for the 2.114 MHz antenna array were placed 76 meters apart and the dipoles were elevated approximately 24 meters above the ground. The poles for the 3.145 MHz antenna array were placed 52 meters apart and the dipoles were elevated approximately 19 meters above the ground. The feed lines of the antenna were connected to coaxial cables originating from the transmitters at the ground center of the array. Balun coils were provided for matching the balance-to-ground feed lines to the unbalanced coaxial cables.

The rocket receiving antenna is a magnetic dipole consisting of two

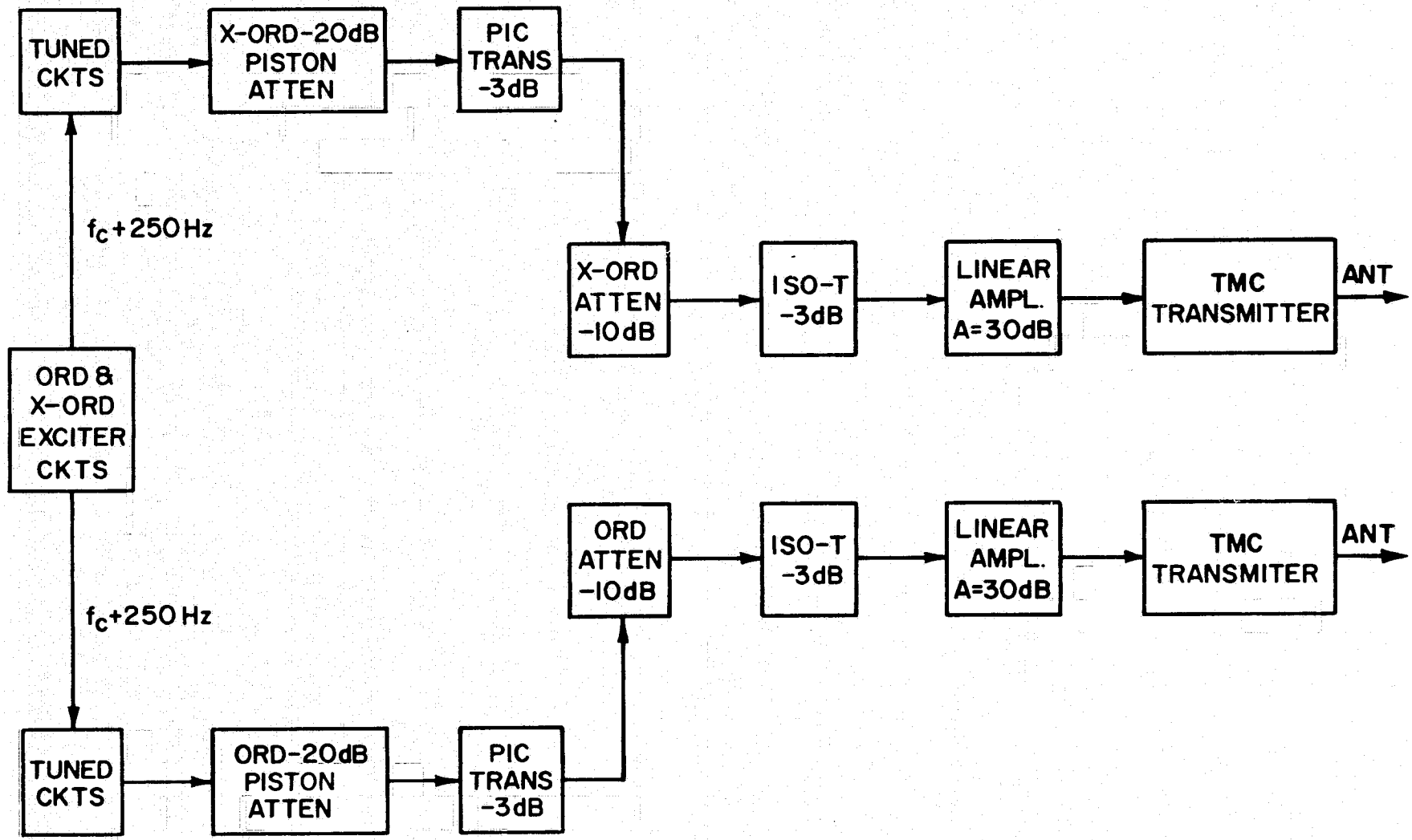

Figure 3.4 Block diagram of the modified system.

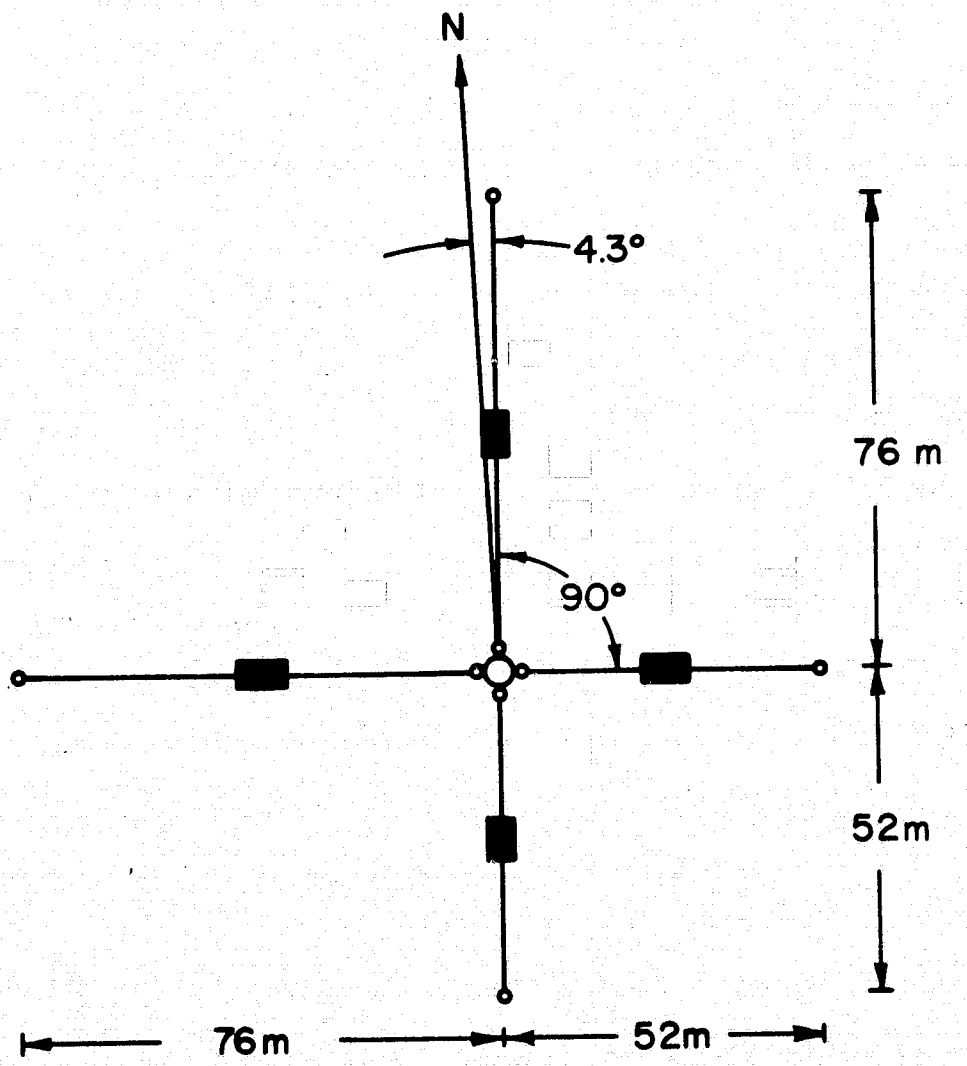

Figure 3.5 Transmitting antenna arrays.

ferrite rods wound with a coil and tuned with a variable capacitor. A one-turn shielded symmetrically link couples the antenna to the receiver with the proper impedance. A schematic diagram of the rocket receiving antenna is shown in Figure 3.6. The antenna assembly is encapsulated in foam and mounted within a fiberglass cylindrical section of the payload as shown in Figure 3.7.

The output of the antenna is fed to a transistorized, crystal controlled receiver designed and developed by G. W. Henry, Jr. [*Edwards*, 1975]. The receiver uses dual-gate MOSFET devices for the RF amplifier, mixer, and three IF amplifier stages. These devices are characterized by a strong immunity to overload effects on strong signals, possess a nearly straight-line logarithmic AGC control characteristic and are gain-temperature independent. The bandpass of the receiver is shown in Figure 3.8 and the AGC and detector characteristics versus input signal level are shown in Figure 3.9. The specifications of the receiver are summarized in Table 3.2. Three completed receivers, one with the cover plates removed to reveal the complete receiver circuitry, are shown in Figure 3.10. The entire receiver assembly consists of two printed circuit cards, one containing the RF section, and one the IF section with input connector, separated by a center metal plate.

3.4 *Payload Description*

The payload contained a dc/Langmuir probe and the radio receivers. The Langmuir probe was mounted on the nosecone tip. The receivers and antennas for the radio-propagation experiment were enclosed in the fiberglass section of the payloads. The payload also contained the spin magnetometer, a 210 kHz tone range receiver and filter, two quadraloop tone ranging antennas and four 30°-turnstile antennas. The four 30°-turnstile antennas

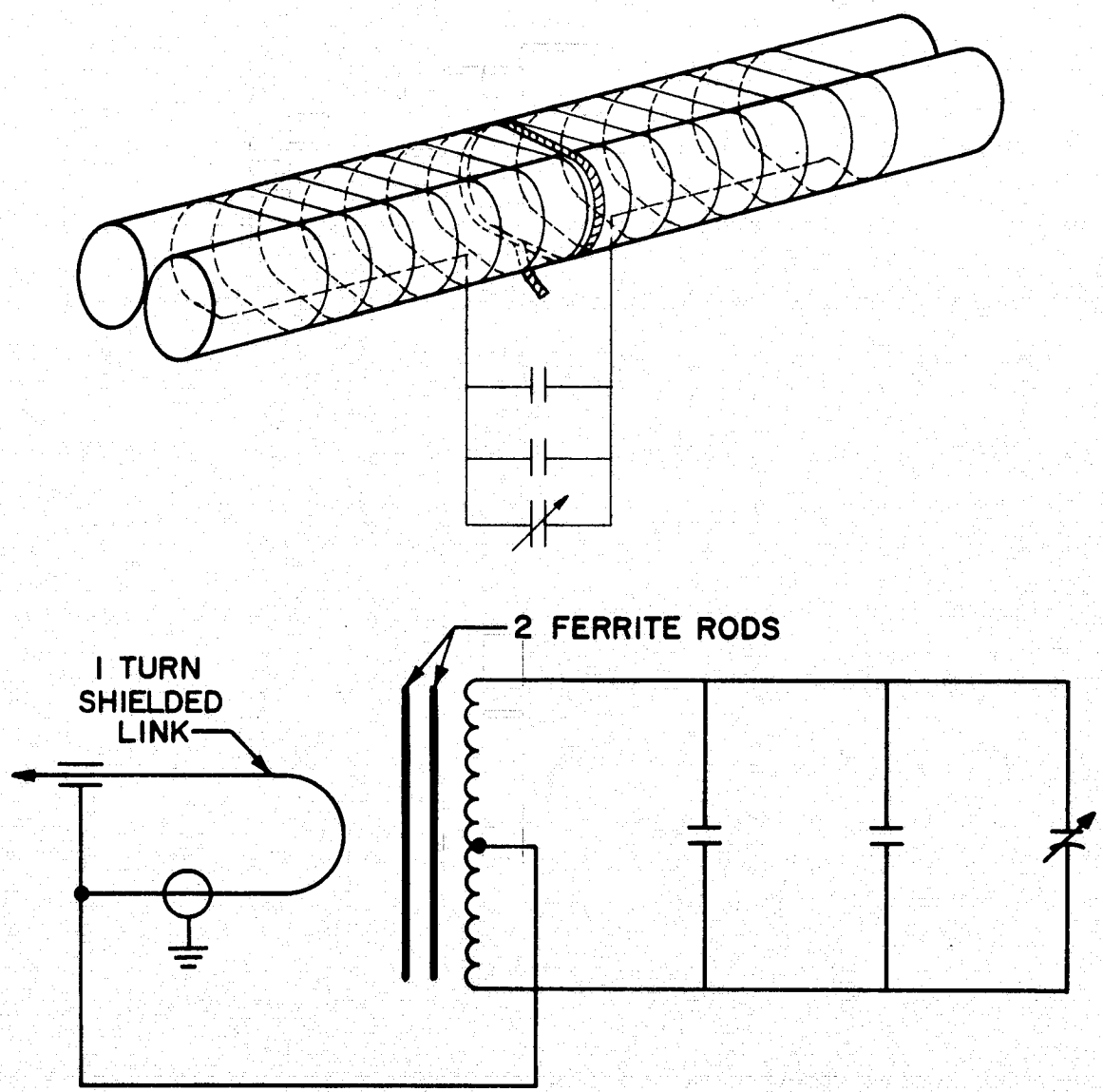

Figure 3.6 Schematic of the rocket receiving antenna.

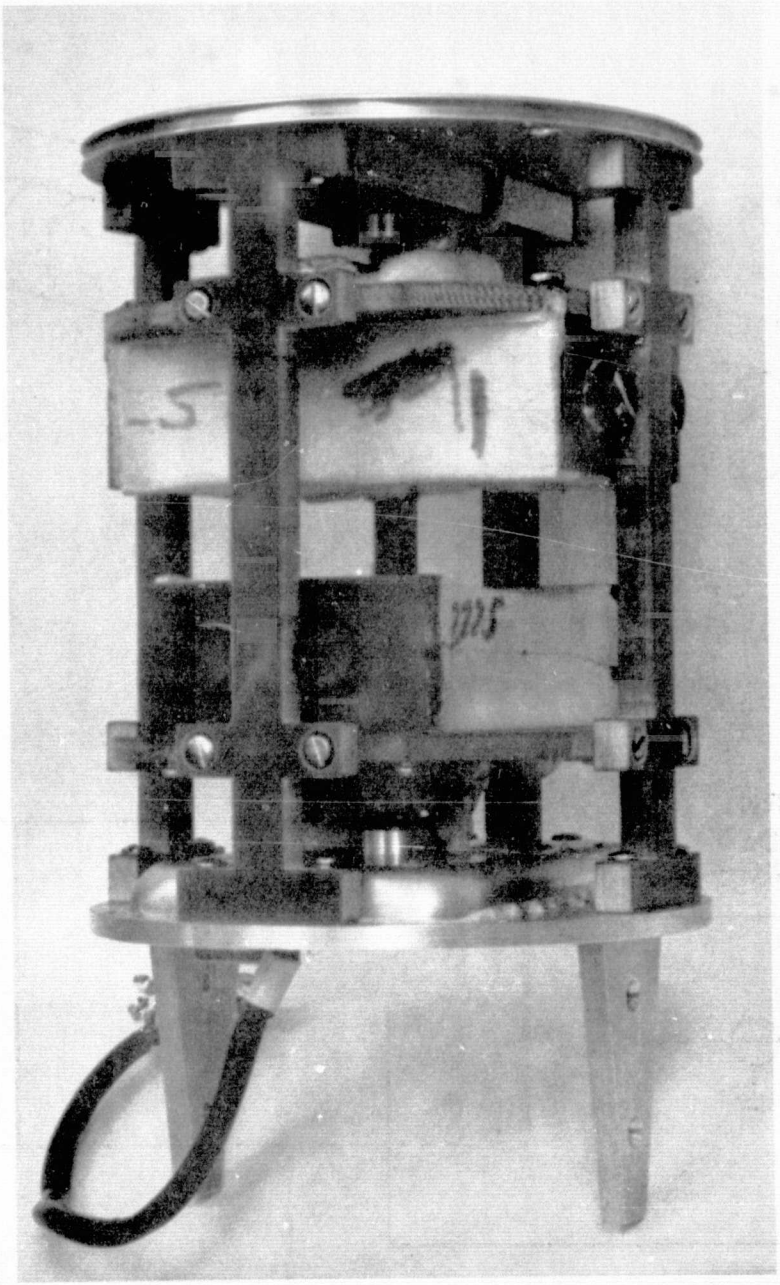

Figure 3.7 Linearly polarized receiving antenna.

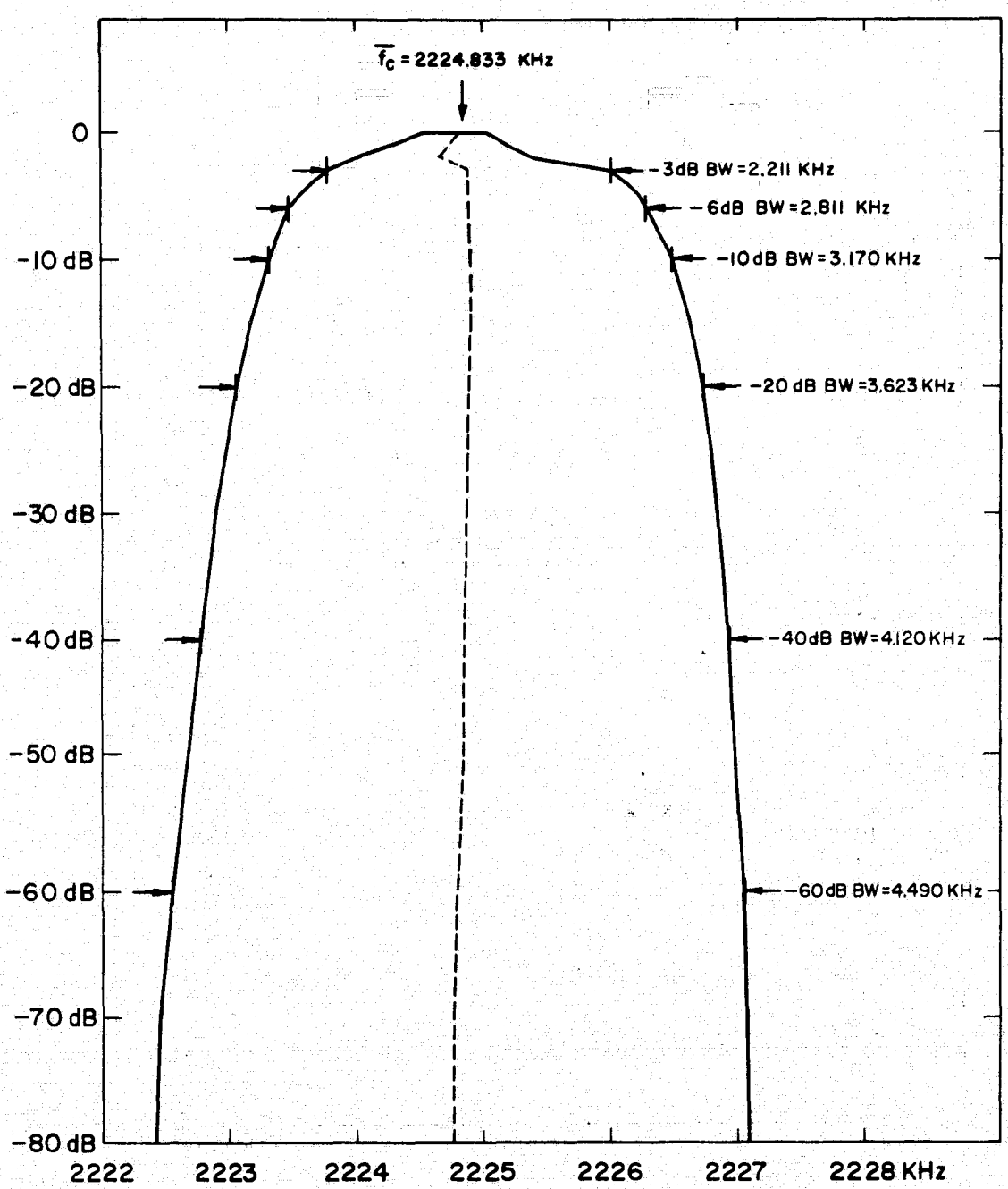

Figure 3.8 IR-1274 receiver No. 1 bandpass characteristics [G. W. Henry, Jr., in *Edwards*, 1975].

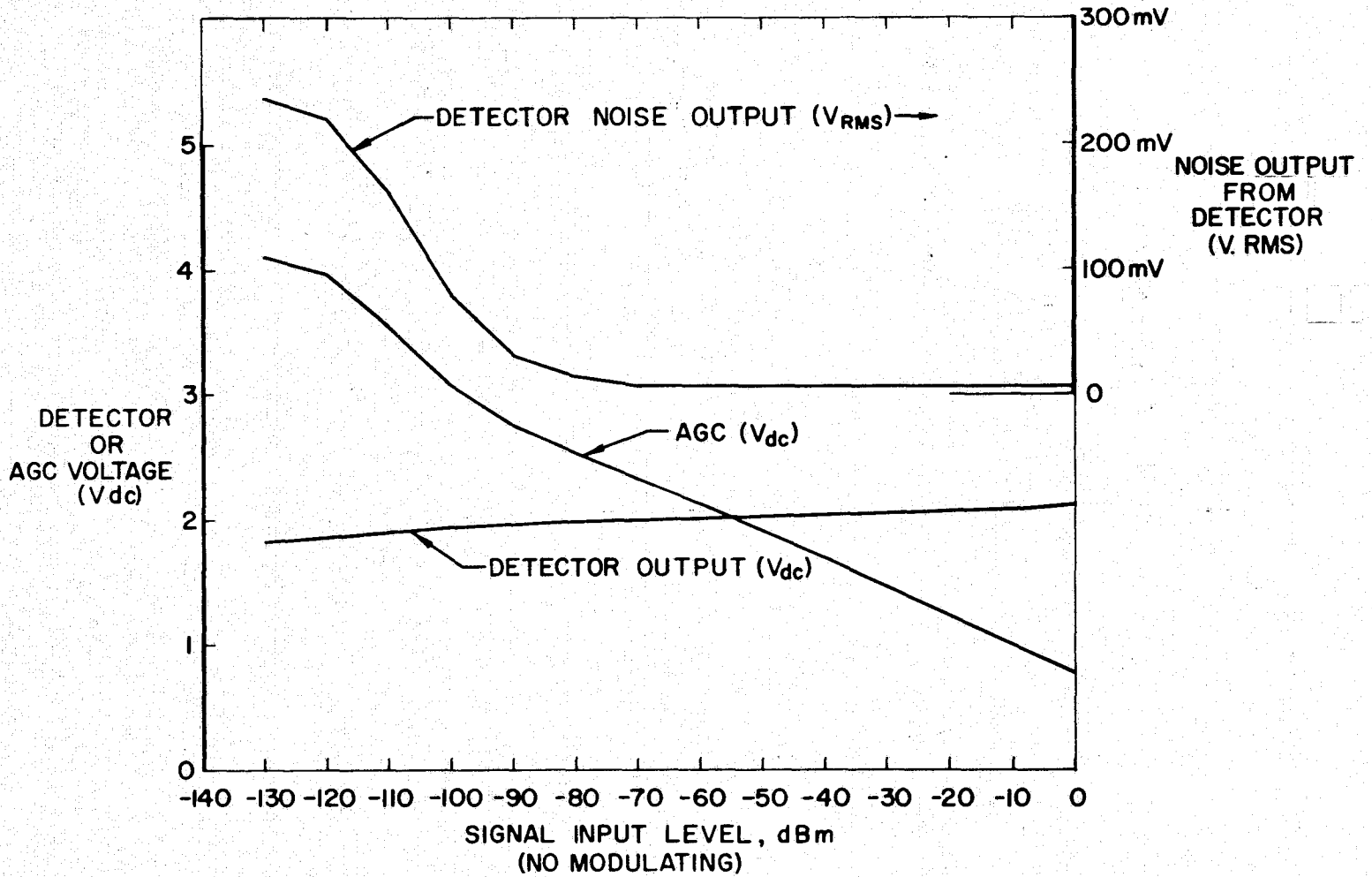

Figure 3.9. Detector characteristics versus input signal level [G. W. Henry, Jr., in *Edwards*, 1975].

TABLE 3.2

IR-1274 receiver performance data.

Input:	Frequency	2.0 to 5.0 MHz
	Level	-110 to + 10 dBm
	Impedance	To match ferrite antenna (600 ohm nominal)
Selectivity:	-6 dB bandwidth	2.811 kHz
	-60 dB bandwidth	4.490 kHz
	Shape factor (60/6)	1.597 : 1
Spurious Responses (for 2.225 MHz f_c): (2.0 to 5.) MHz range)		2122 kHz -103 dB 2156 kHz -103 dB 2451 kHz -102 dB 2470 kHz -100 dB 3135 kHz - 50 dB (Image)
AGC Characteristics:		
	Detector Output Flatness	±0.2 volt, -110 to +10 dBm input
	AGC Voltage Range:	+5.0 volts (minimum signal) 0.8 volt (maximum signal)
	AGC Output Impedance	2.2 kΩ or kiloohms
Detector Characteristics:		
	Nominal dc Output	2.0 ± 0.2 volts
	Linearity	±2 dB, 0.15 to 4.0 volts
	Temperature Stability (-10 to +50°C)	Gain: ± 3 dB Offset: ± 0.05 volt
	Output Impedance	Less than 10 ohms
Power Requirements:		+20 to +35 volts @ 55 mA -20 to -35 volts @ 15 mA
Environment:		
	Temperature	-10 to +50°C
	Shock and Vibration	0 to 15 g, sinusoidal 30g, random

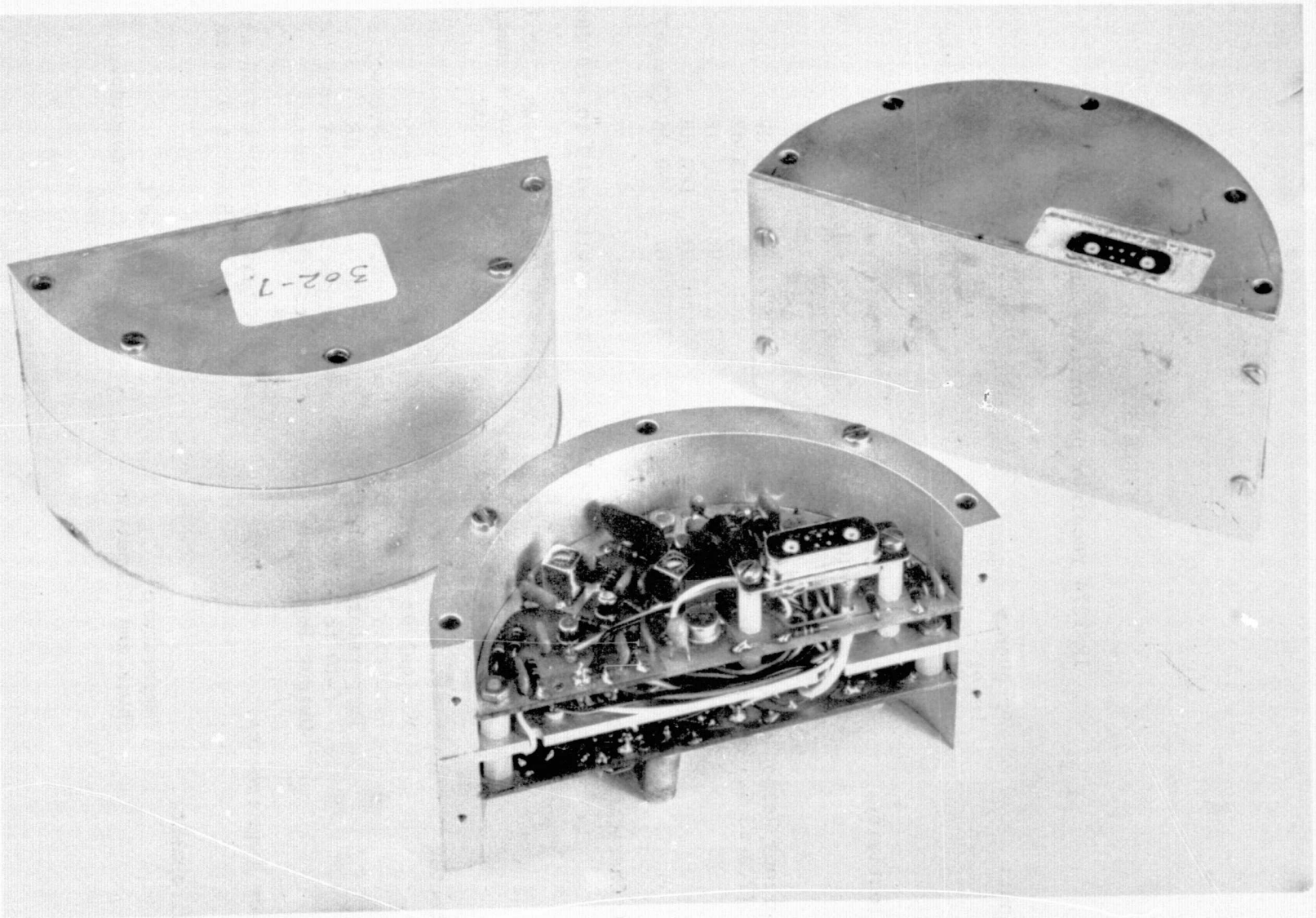

Figure 3.10 Three completed receivers, one with cover plates removed.

were located at the base of the payload. The two quadraloop tone ranging antennas were located directly in front of the turnstile.

Nike Apache 14.532 included two additional probe experiments for measuring electron temperature. These probes were mounted on two deployable booms. One of these probes duplicated the boom-mounted probe flown successfully on Nike Apaches 14.475, 14.476, 14.513 and 14.514 [*Schutz et al.*, 1975]. The other probe was an RF resonance probe supplied by Dr. K. Hirao and Dr. K. Oyama from the University of Tokyo.

The dc/Langmuir probe was modified in this payload to observe the fine structure of the electon concentration profile [L. G. Smith in *Edwards*, 1975]. The modifications in the instrumentation were suggested by *Prakash et al.* [1972] whose experiment was a direct adaptation of the dc-probe experiment developed by *Smith* [1967]. In the dc-probe experiment the current to the nose tip electrode is measured at a fixed voltage. An electrometer with a diode in the feedback loop is used to give a logarithmic scale of current over six decades, from 10^{-10} A to 10^{-4} A. The output of the logarithmic electrometer is telemetered to the ground where it is recorded on magnetic tape.

To examine the structure of the ionosphere with greater resolution, both in altitude and electron concentration, the ac component of the electrometer output signal was amplified and telemetered to the ground on a separate channel. The amplitude of this signal is proportional to the fractional change in electron concentration. The circuit of the ac amplifier used in the Peru launches is shown in Figure 3.11. With this modification we can measure the fractional change in electron concentration to 0.1%.

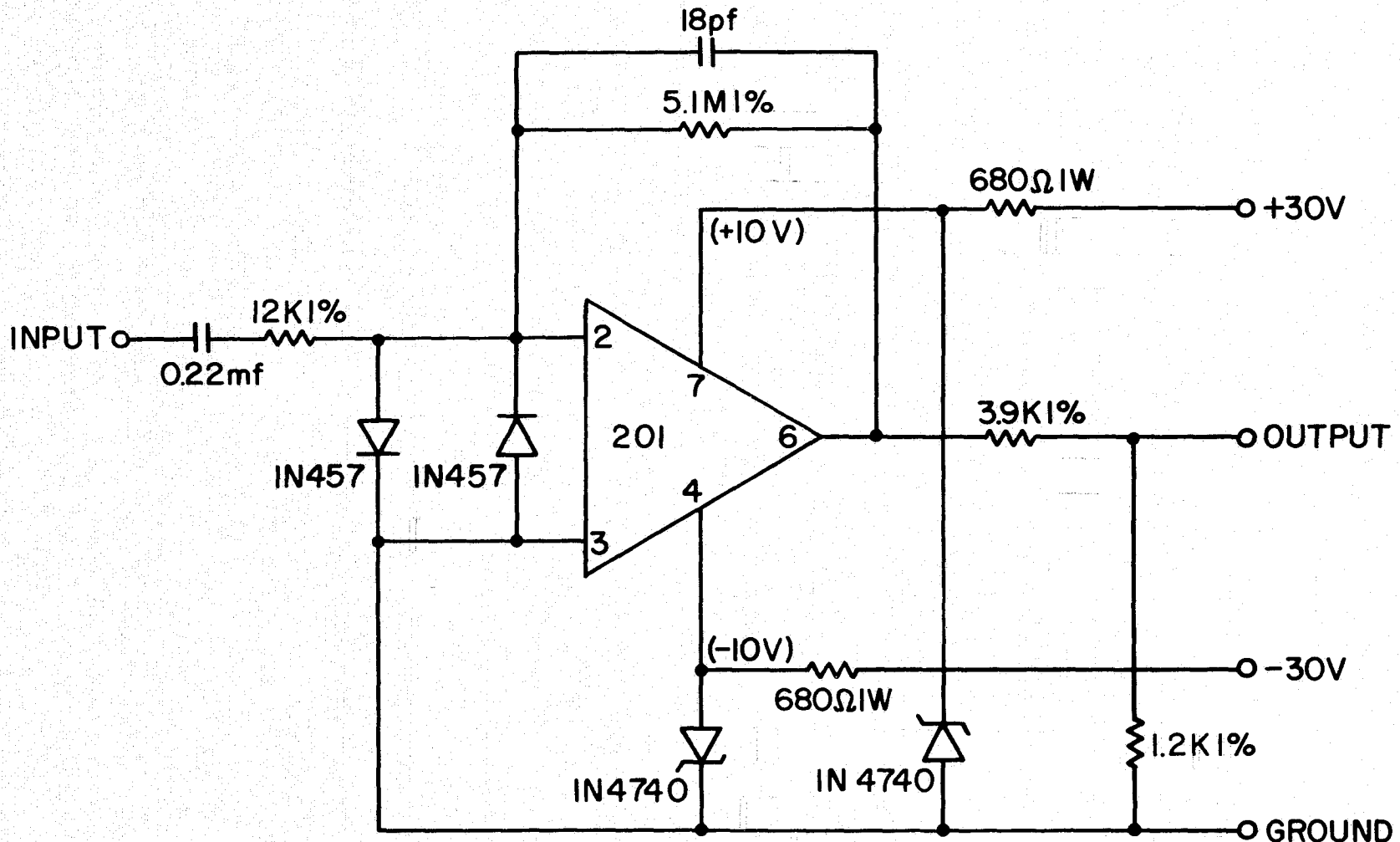

Figure 3.11. AC amplifier for electron-density fine-structure experiment [L. G. Smith, in *Edwards*, 1975].

4. DATA ANALYSIS

4.1 *An Algorithm for Determining the Spectra of Finite Length Discrete Time Sequences*

The problem under consideration here is the determination of the frequencies, f_j (3.15), of the principal relative maxima, M_j, of the amplitude spectra of finite length discrete time sequences. The discrete Fourier transform (DFT) [*Bergland*, 1969] of a finite length discrete time sequence can be calculated by the fast Fourier transform (FFT) [*International Mathematical and Statistical Libraries, Inc.*, 1975.] Although most of the properties of the continuous Fourier transform (CFT) are retained, several differences result from the constraint that the FFT must operate on a limited number of discrete samples. The errors most often encountered in using the FFT are aliasing and leakage [*Bergland*, 1969]. In order to determine the f_j's accurately, aliasing and leakage errors must be minimized.

The term aliasing refers to the distortion in the amplitude spectrum of a signal by the appearance of high frequency components as low frequency components. This error occurs as a result of sampling at a rate less than the Nyquist sampling rate, f_{Ns}. The Nyquist sampling rate is the sampling rate at which a continuous function $g(t)$ can be uniquely recovered from its sampled version

$$\hat{g}(t) = \sum_{n=-\infty}^{\infty} g(nT)\,\delta(t-nT) \tag{4.1}$$

where $T = 1/f_{Ns}$ [*Brigham*, 1974]. In particular, $g(t)$ is given by

$$g(t) = T \sum_{n=-\infty}^{\infty} g(nT)\ \sin \frac{\{\pi f_{Ns}(t-nT)\}}{\pi(t-nT)} \tag{4.2}$$

To eliminate aliasing one simply samples at a rate greater than the Nyquist sampling rate (e.g., sample at a rate greater than twice the highest frequency component present).

The leakage error is related to the way in which a finite-length signal is formed from a long-duration signal. Multiplication of the signal in the time domain by a rectangular window is equivalent to convolving the amplitude spectrum of the rectangular window with the spectrum of the long-duration signal. For simplicity, we chose a cosine waveform of constant frequency, f_c, to illustrate the concept of leakage in Figure 4.1. Notice that the resultant amplitude spectrum is not restricted to one frequency, f_c, but in fact has a series of small sidelobes. The occurrence of these undesirable sidelobes is called leakage.

Although leakage is an inherent error in the Fourier analysis of any finite-length signal, it can be reduced significantly by utilizing a time domain window which has small sidelobes in the frequency domain. Several examples of windows which have been used by others [*Oppenheim and Schafer*, 1975; *Blackman and Tukey*, 1958] to reduce leakage are the

(1) Bartlett window

$$W(n) = \begin{cases} \frac{2n}{L-1} & , \quad 0 \leq n \leq \frac{L-1}{2} \\ 2 - \frac{2n}{L-1} & , \quad \frac{L-1}{2} \leq n \leq L-1 \end{cases} \tag{4.3}$$

where n and L are integers,

(2) Hanning window

$$W(n) = \frac{1}{2}\left[1-\cos\left(\frac{2\pi n}{L-1}\right)\right] \ , \ 0 \leq n \leq L-1 \tag{4.4}$$

(3) Hamming window

$$W(n) = .54 - .46 \cos\left(\frac{2\pi n}{L-1}\right) \ , \quad 0 \leq n \leq L-1 \tag{4.5}$$

and (4) Blackman window

$$W(n) = .42 - .50 \cos\left(\frac{2\pi n}{L-1}\right) + .08 \cos\left(\frac{4\pi n}{L-1}\right) \ , \ 0 \leq n \leq L-1 \tag{4.6}$$

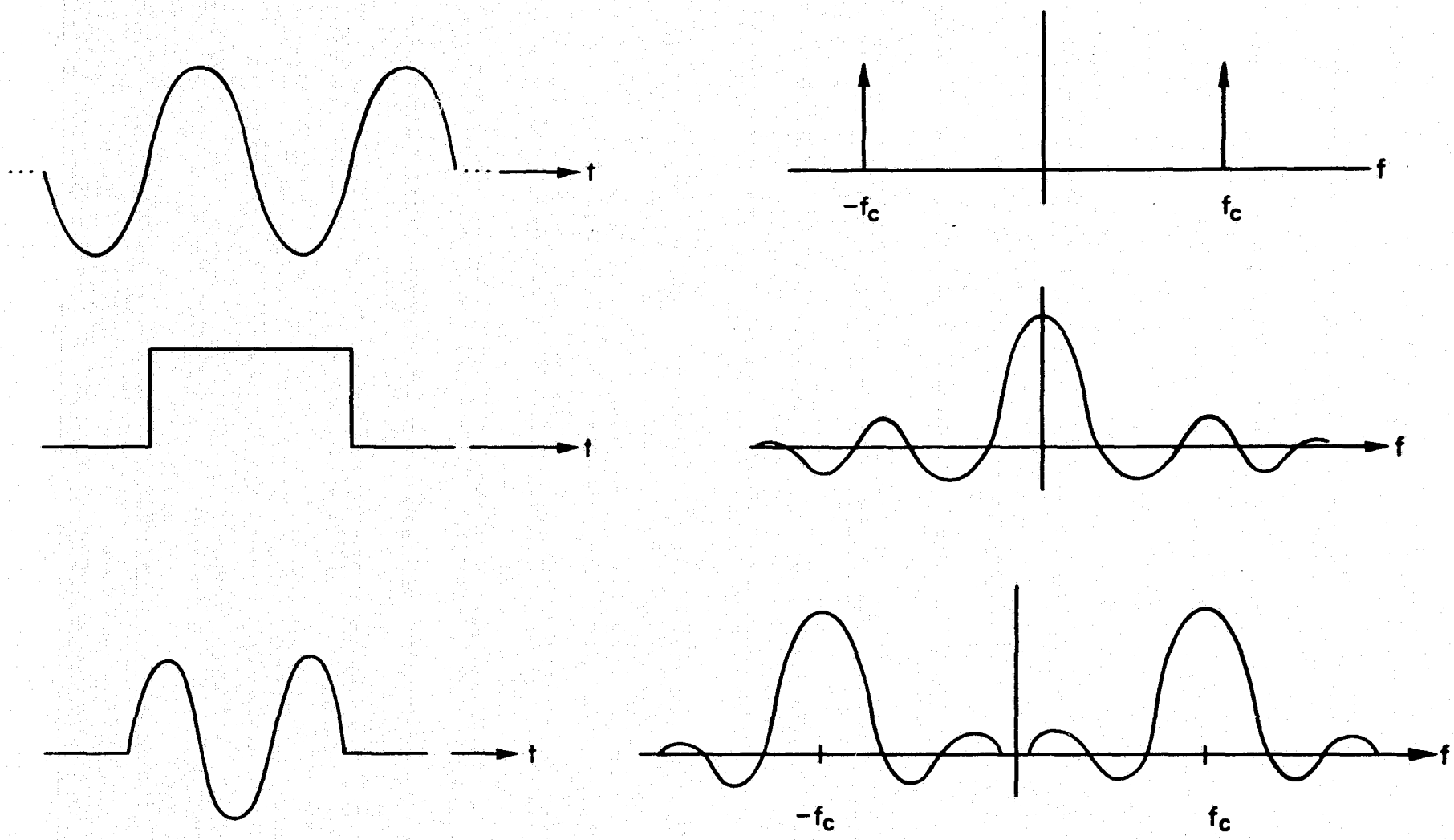

Figure 4.1 Rocket receiver output, and the corresponding magnetometer output [P. E. Monro, in *Edwards*, 1974].

While each of these windows reduces leakage to some extent, a better window has been chosen for the present application.

The Fourier transform of a Gaussian function is another Gaussian function. Thus, a Gaussian window eliminates leakage because it has no sidelobes in the frequency domain.

The amplitude spectrum of the rocket receiver signal after windowing is Gaussian within a symmetric neighborhood of the f_j's. This is illustrated in Figure 4.2. Utilizing this result, E. K. Walton has suggested an algorithm which accurately determines the frequencies of the principal relative maxima of the receiver output containing the Faraday rotation rate.

Consider the Gaussian curve

$$X' = A \exp \{-\alpha(f-f_j)^2\} \tag{4.7}$$

shown in Figure 4.3, where A and α are constants, and f_j is any one of the frequencies of equation (3.15). Given three points on this Gaussian curve

$$(f_{k-1}, X'_{k-1}), (f_k, X'_k), (f_{k+1}, X'_{k+1})$$

where X'_{k-1}, X'_k, X'_{k+1} are the amplitudes of the frequency components f_{k-1}, f_k and f_{k+1}, respectively, and we wish to determine f_j. First compute the natural logarithm of X'_k/X'_{k+1} and X'_k/X'_{k-1}.

$$\ell n \frac{X'_k}{X'_{k+1}} = \ell n \frac{A \exp \{-\alpha(f_k-f_j)^2\}}{A \exp \{-\alpha(f_{k+1}-f_j)^2\}} \tag{4.8}$$

$$\ell n \frac{X'_k}{X'_{k+1}} = -\alpha(f_k-f_j)^2 + \alpha(f_{k+1}-f_j)^2 \tag{4.9}$$

Similarly,

$$\ell n \frac{X'_k}{X_{k-1}} = -\alpha(f_k-f_j)^2 + \alpha(f_{k-1}-f_j)^2 \tag{4.10}$$

Dividing equation (4.3) by (4.4) yields

$$G = \frac{-(f_k-f_j)^2 + (f_{k+1}-f_j)^2}{-(f_k-f_j)^2 + (f_{k-1}-f_j)^2} \tag{4.11}$$

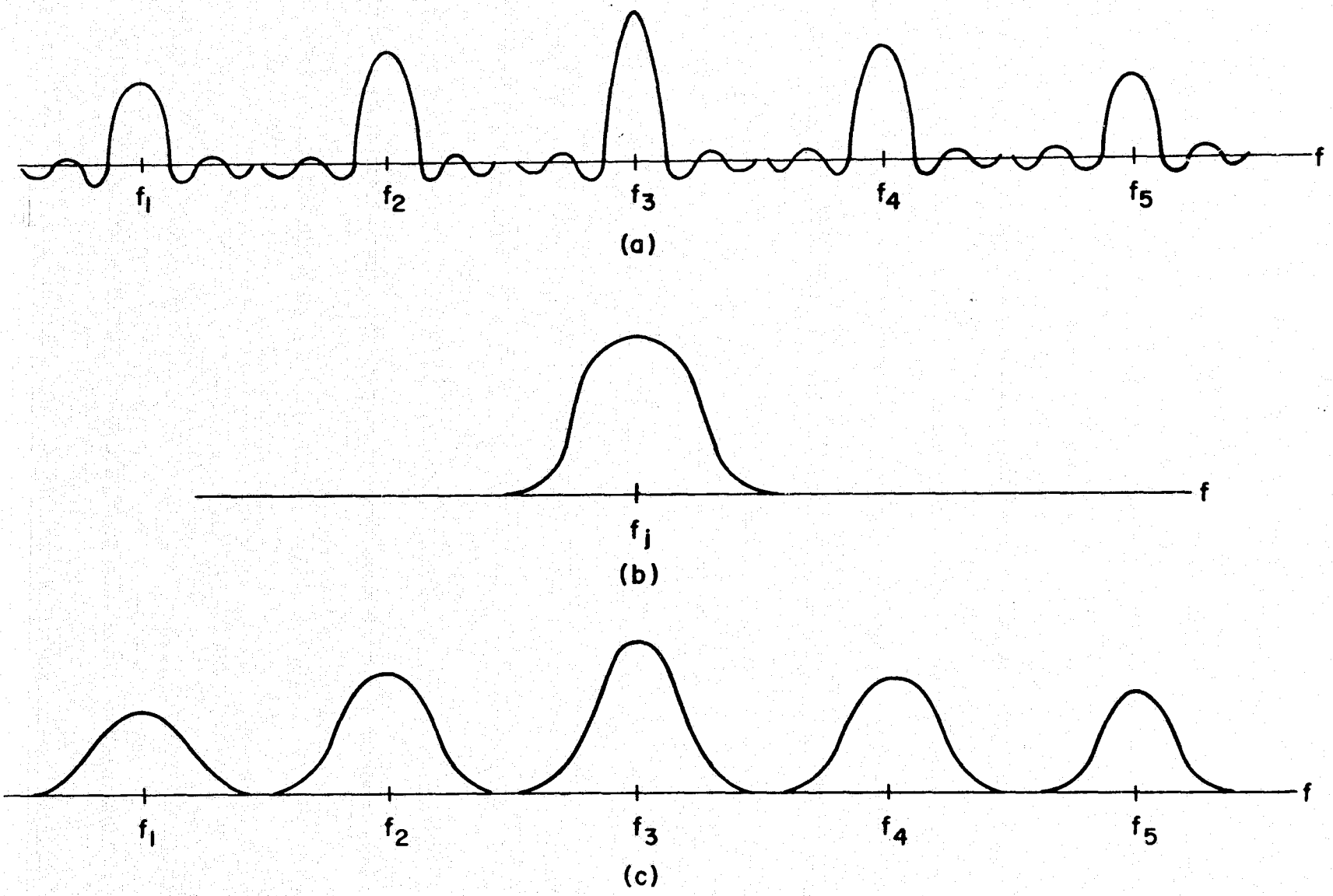

Figure 4.2 (a) Amplitude spectrum of rocket receiver signal, (b) amplitude spectrum of Gaussian window, (c) convolution of (a) and (b).

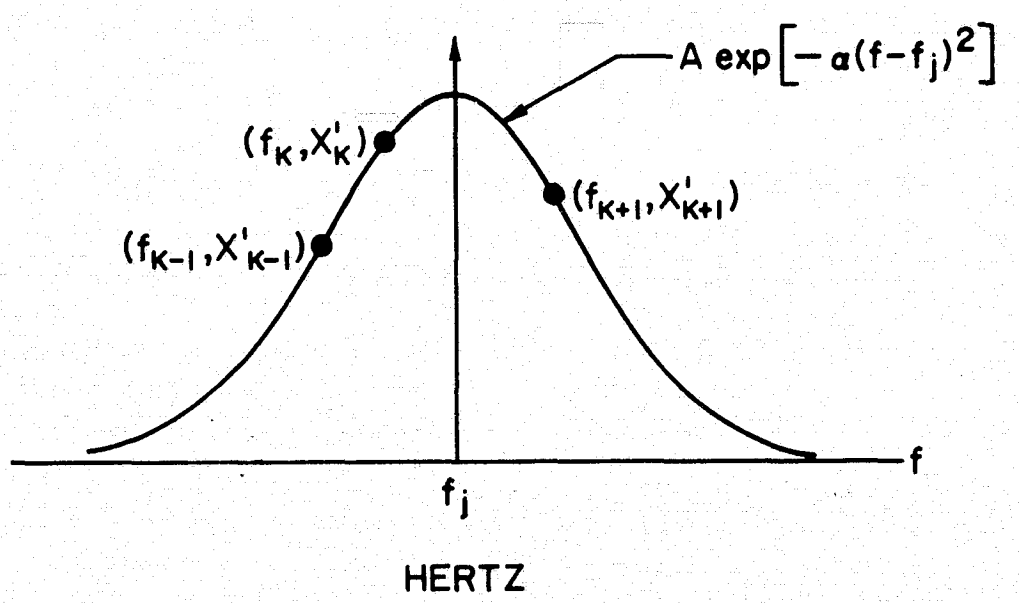

Figure 4.3 Gaussian curve.

where

$$G = \frac{\ell n(X_k/X_{k+1})}{\ell n(X_k/X_{k-1})} \tag{4.12}$$

Expanding the numerator and denominator of equation (4.11) and simplyfing yields

$$G = \frac{f_{k+1}^2 - 2f_{k+1}f_j - f_k^2 + 2f_kf_j}{f_{k-1}^2 - 2f_{k-1}f_j - f_k^2 + 2f_kf_j} \tag{4.13}$$

Multiplying both sides of equation (4.13) by the denominator on the right side of equation (4.13) one obtains

$$G(f_{k-1}^2 - f_{k-1}f_j - f_k^2 + 2f_kf_j) = f_k^2 - 2f_{k+1}f_j - f_k^2 + 2f_kfj \tag{4.14}$$

Solving for f_j yields

$$f_j = \frac{f_{k+1}^2 - f_k^2 - G(f_{k+1}^2 - f_k^2)}{2G(f_k - f_{k-1}) - 2(f_k - f_{k+1})} \tag{4.15}$$

Since the FFT algorithm calculates the Fourier coefficients of the Gaussian curve for every integer frequency, equation (4.15) can be simplified. Let

$$f_k = k,\ f_{k-1} = k-1, \text{ and } f_{k+1} = k+1$$

then equation (4.15) reduces to

$$f_j = k + \frac{1}{2}\ \frac{1-G}{1+G} \tag{4.16}$$

Before the algorithm was applied to rocket data, it was tested on several computer-generated sinusoidal signals of various input frequencies, f_c, and phases, ϕ. The specific sinusoids and the results, f_j, of their processing are shown in Tables 4.1 and 4.2. The sinusoids listed in Table 4.2 had been previously processed by an algorithm written by K. L. Miller [*Edwards*, 1975]. Miller's algorithm uses a rectangular window in the time domain which does not minimize leakage. Tables 4.1 and 4.2 show that algorithm (4.14) reduces leakage such that the maximum error in recovering the frequency of the input sinusoid is less than ± .0025 Hz. The computer program for implementing this algorithm is given in Appendix I.

TABLE 4.1

Test #1 of algorithm 4.14.

	f_c *	f_j **	$f_j - f_c$
#1	7.350	7.35185	.00185
#2	7.350	7.35162	.00162
#3	7.350	7.35187	.00187
#1	7.31416	7.31633	.00217
#2	7.31416	7.31607	.00191
#3	7.31416	7.31635	.00219
#1	503.5	503.49976	-.00024
#2	503.5	503.49976	-.00024

*Computer generated sinusoids

#1 $\sin\left(\frac{2\pi f_c N}{6000}\right)$; $N = 1, 2, \ldots, 6000$

#2 $\sin\left(\frac{2\pi f_c N}{6000} + \frac{\pi}{6}\right)$; $N = 1, 2, \ldots, 6000$

#3 $\sin\left(\frac{2\pi f_c N}{6000}\right)$; $N = 10, 20, \ldots, 6000$

**Found by algorithm 4.14

TABLE 4.2

Test #2 of algorithm 4.14.

Phase, ϕ (Degrees)	f_j *	f_j **
0	7.00002	6.978
10	7.00002	6.980
20	7.00001	6.984
30	7.00001	6.989
40	7.00000	6.996
50	6.99999	7.004
60	6.99998	7.011
70	6.99997	7.016
80	6.99997	7.020
90	6.99997	7.020
100	6.99997	7.020

Computer generated sinusoids

$$\sin\left(\frac{2\pi f_c N}{6000}\right) + \phi \quad ; \quad N = 1, 2, \ldots, 6000$$

$$f_c = 7.00 \text{ Hz}$$

* Found by algorithm 4.14

** Found by Miller algorithm

4.2 *Data Tapes*

Digital data tapes for Nike Apache 14.532 were provided by D. E. Hoskinson, of the NASA Wallops Flight Center Telemetry Section. A catalog of these post-flight tapes is given in Appendix II. Each tape begins with four header records which contain identification information. The next five records, of 1005 words each, give the calibrations of telemetry discriminators. The subsequent records are data records of 2008 words each. Words 0006 through 2005 are data samples. Words 2006, 2007, and 2008 express the universal time of the first data sample of the next record. The time is coded as outlined in Table 4.3.

The original telemetry data from Peru were recorded on analog tapes. The post-flight digital tapes were generated at the Wallops Flight Center from the original analog tapes. To maintain accurate synchronization of time between the analog and digital tapes, a 100 kHz reference signal, recorded on the analog tape during the flight, was used to trigger the analog-to-digital converter. By dividing the 100 kHz reference by four, each of the five channels could be sampled at a rate of 5 kHz in synchronization and faster than the Nyquist rate (approximately 1 kHz) in a simple way. The circuit designed for this purpose by L. J. Johnson of the Aeronomy Laboratory is shown in Figure 4.4.

4.3 *Faraday Rotation*

The Faraday rotation rates were extracted from the radio-propagation data by applying algorithm (4.14) to the receiver and reference signals. In the processing of these signals a Gaussian window of the form

$$W(\ell) = \exp(-.5\delta^2) - C_f \qquad (4.17)$$

where

$$\delta \equiv 3\left(1.0002 - \frac{\ell}{2500}\right) \; ; \; \ell = 1, 2, \ldots, 2500$$

TABLE 4.3

Coding of time words

Word 2006	bits	
	13 - 16	hundreds of milliseconds
	9 - 12	tens of milliseconds
	5 - 8	ones of milliseconds
	1 - 4	tenths of milliseconds

Wood 2007	bits	
	13 - 15	tens of minutes
	9 - 12	ones of minutes
	5 - 7	tens of seconds
	1 - 4	ones of seconds

Word 2008	bits	
	15 - 16	hundreds of days
	11 - 14	tens of days
	7 - 10	ones of days
	5 - 6	tens of hours
	1 - 4	ones of hours

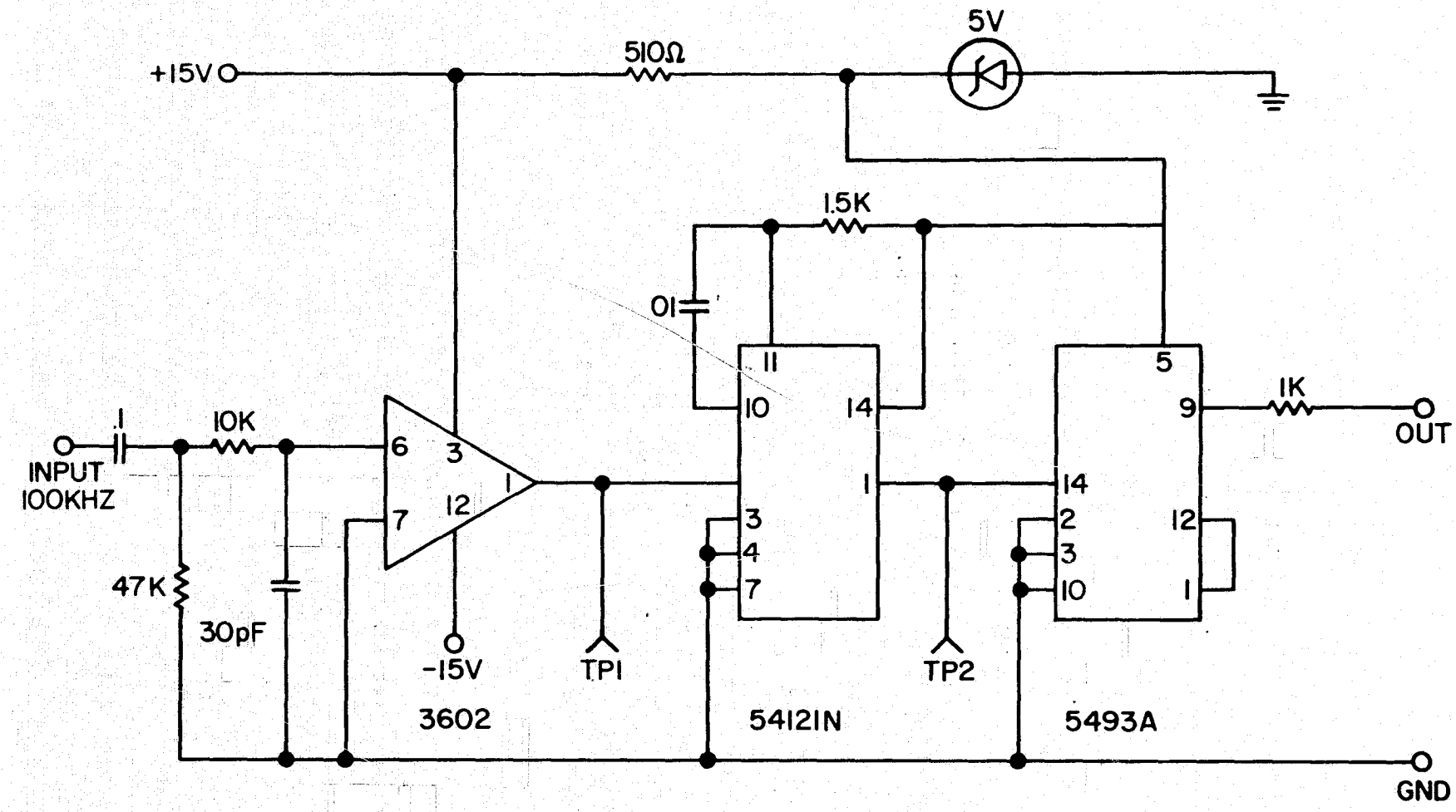

Figure 4.4 Time synchronization circuit.

and

$$C_f = .01111$$

was employed to reduce leakage. The factor C_f was introduced to shift the Gaussian window downward so that the endpoints would lie on the absccia as shown in Figure 4.5. A one-second window was employed to simplify the computer processing.

In Section 3.2 we derived an approximate expression for the receiver output under ideal conditions, equation (3.8). The frequencies of the principal relative maxima of the amplitude spectrum containing the Faraday rotation rate were given by f_1, f_2, f_3, f_4, and f_5. Since f_3 is independent of the rocket spin rate, f_s, any change in f_s will appear only in f_1, f_2, f_4, and f_5. Therefore, f_3 provides a reference for identifying f_1, f_2, f_3, f_4, and f_5 in the spectrum. For example, consider the amplitude spectra of the 3 MHz receiver output of Nike Apache 14.532 before and after the deployment of the boom probes as shown in Figure 4.6. The principal relative maxima corresponding to frequencies f_1, f_2, f_3, f_4, and f_5 are labeled M_1, M_2, M_3, M_4 and M_5 in Figure 4.6. Since the deployment of the boom probes decreases the rocket spin rate, M_1, M_2, M_4, and M_5 are closer in frequency to M_3 after the deployment of the boom probes as illustrated in Figure 4.6.

The measured quantities f_1, f_2, f_3, f_4, f_5, f_R, and f_s may be combined in many different ways to determine f_F. For example,

$$f_F = f_3 - f_R \tag{4.18}$$

$$f_F = f_1 - f_R + 4f_s \tag{4.19}$$

$$f_F = f_2 - f_R + 2f_s \tag{4.20}$$

$$f_F = f_4 - f_R - 2f_s \tag{4.21}$$

$$f_F = f_5 - f_R - 4f_s \tag{4.22}$$

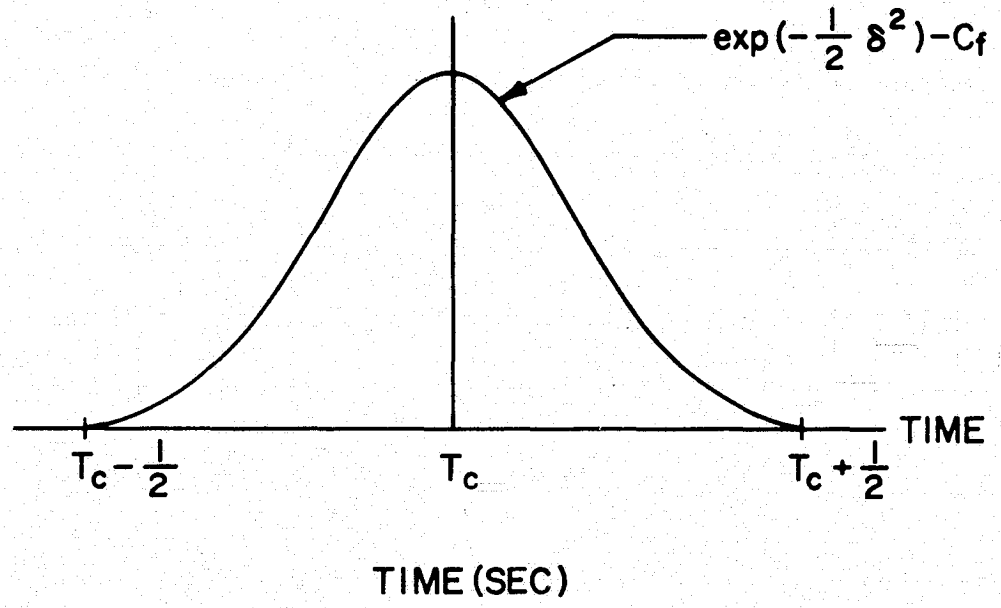

Figure 4.5 The Gaussian window T_c ≡ center time.

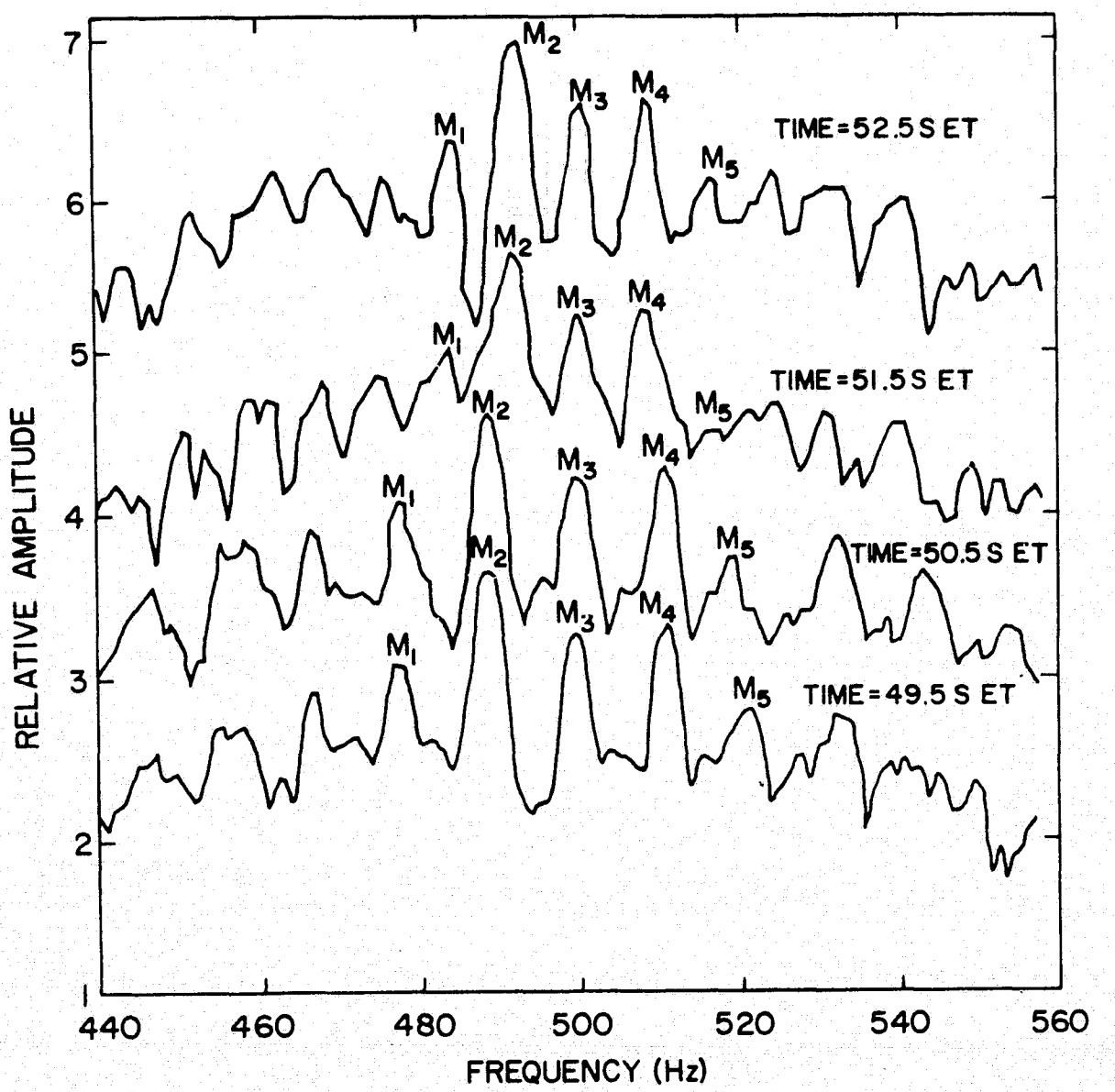

Figure 4.6 Amplitude spectra of 3 MHz receiver for Nike Apache 14.532 before and after deployment of boom probes (i.e., 51.1 S ET).

$$f_F = \frac{f_1+f_5}{2} - f_R \tag{4.23}$$

$$f_F = \frac{f_2+f_4}{2} - f_R \tag{4.24}$$

are seven different expressions for calculating f_F. Although equation (4.18) is the simplest expression for calculating f_F, f_3 contains a larger error produced by cross talk between the data lines. Utilizing either equation (4.19), (4.20), (4.21), or (4.22) to calculate f_F requires a knowledge of f_s in addition to f_R. Since the receiver and aspect magnetometer outputs contain a large dc component, their amplitude spectra are not Gaussian within a 6 Hz symmetric of the spin rate. Therefore, f_s cannot be accurately determined from the lower portion of the receiver spectrum or the aspect magnetometer spectrum. While f_s can be determined by algebraically combining f_1 or f_2 with either f_4 or f_5, equations (4.23) and (4.24) offer a simpler alternative for calculating f_F. While equations (4.23) and (4.24) are algebraically similar, equation (4.23) contains a large error component. This result is illustrated in Figure 4.7. Figure 4.7 is a plot of f_s versus elapsed time, in which f_s was determined by algebraically combining f_1 and f_2 with f_4 and f_5. The large error in f_5, illustrated by the large fluctuations in f_s determined by algebraically combining f_5 with f_1 and f_2, is the major source of error in equation (4.23). Therefore, equation (4.24) was used to calculate f_F.

The frequencies f_1, f_2, f_3, f_4, f_5, and the corresponding reference frequencies and Faraday rotation rates for the 3 MHz radio-propagation experiment of Nike Apache 14.532 during the period from 70.5 to 77.0 seconds are given in Tables 4.4 and 4.5. No reliable Faraday rotation rates were obtained before 72 or after 75 seconds.

The method of analysis [*Mechtly et al.*, 1970] based on the complete

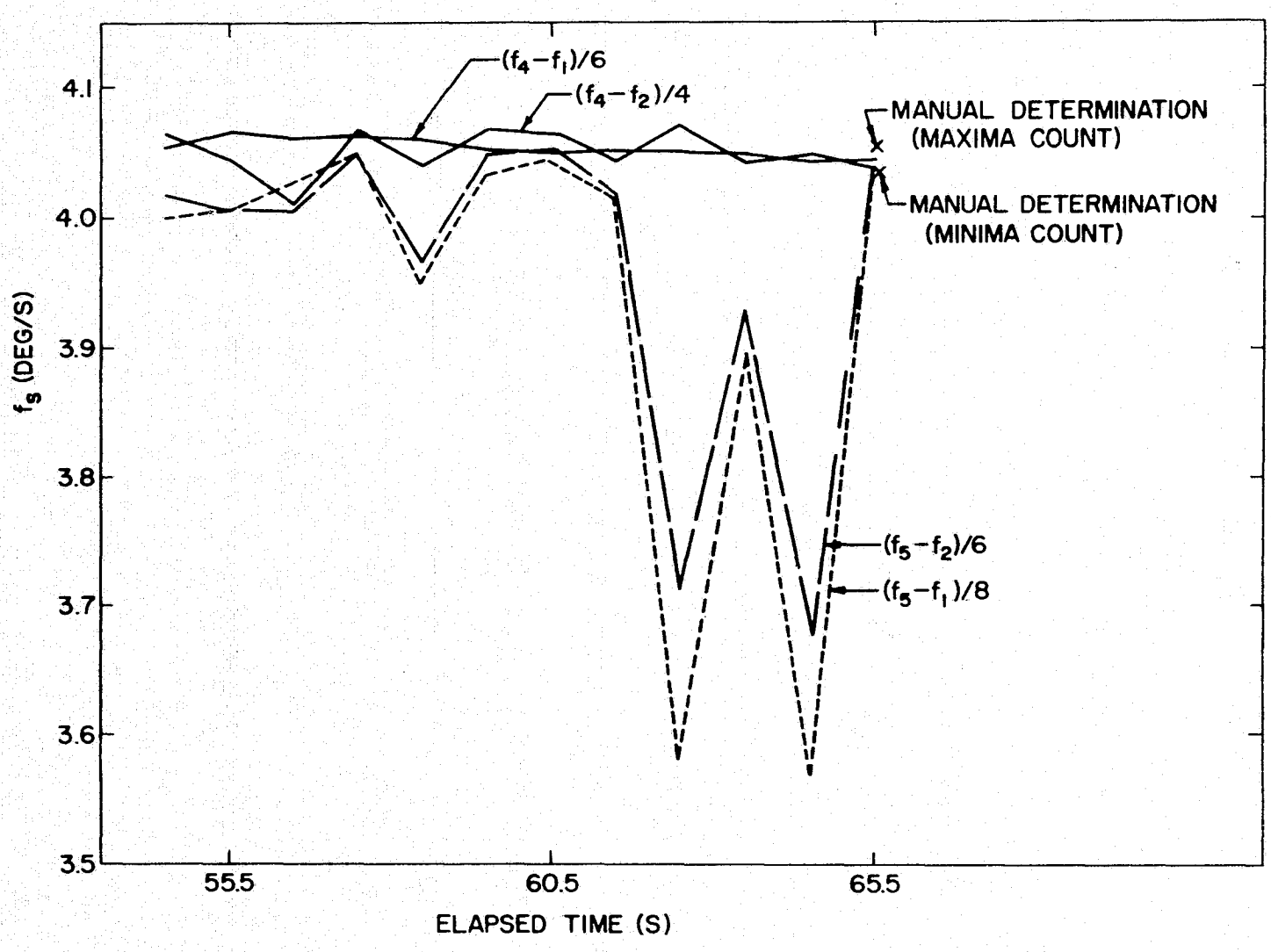

Figure 4.7 Plot of f_s versus time as calculated from combinations of f_1, f_2, f_4, and f_5.

TABLE 4.4

Frequencies f_1, f_2, f_3, f_4, and f_5 for the 3 MHz radio-propagation experiment from Nike Apache 14.532.

Elapsed time (seconds)	f_1	f_2	f_3	f_4	f_5
70.5	484.1306	492.41772	500.41187	508.66772	520.77930
71.0	484.20313	492.50122	500.60815	508.77734	520.03027
71.5	484.57910	492.49512	500.58813	508.67505	519.47241
72.0	484.35791	492.49658	500.52686	508.74756	520.57861
72.5	484.52246	492.49536	500.63306	508.70752	519.51074
73.0	484.34521	492.46777	500.54761	508.73218	
73.5	484.35181	492.47119	500.51587	508.77222	518.97437
74.0	484.08081	492.46265	500.46265	508.82715	
74.5	483.00000	492.45947	500.58203	508.81689	
75.0	485.54980	492.45850	500.47632	508.77002	
75.5		492.27661	500.49585	508.72559	
76.0	485.90576	491.86963	500.59277	508.72144	520.98535
76.5		492.53223	500.56079	508.82617	
77.0		492.19604	500.47046	508.80420	
77.5		492.41162	500.38013		
78.0		492.39453	500.69238	508.90430	

TABLE 4.5

Reference frequencies and Faraday rotation rates for 3 MHz radio-propagation experiment from Nike Apache 14.532.

Elapsed Time	f_R (Hz)	$\frac{f_2+f_4}{2} - f_R$ (Hz)	f_F (Hz)	f_F (deg/sec)
70.5	500.51147	500.54272	.03125	11.2500
71.0	500.57861	500.63928	.06067	21.8412
71.5	500.59106	500.58509	-.32551	-117.1836
72.0	500.58789	500.62207	.03418	12.3048
72.5	500.58618	500.60144	.01526	5.4936
73.0	500.58569	500.59998	.01429	5.1444
73.5	500.58472	500.62171	.03699	13.3164
74.0	500.58105	500.64490	.06385	22.9860
74.5	500.57935	500.63818	.05883	21.1788
75.0	500.57739	500.61426	.03687	13.2732
75.5	500.57422	500.50110	-.06322	-22.7592
76.0	500.57056	500.29554	-.27502	-99.0072
76.5	500.56665	500.67920	.11255	40.5180
77.0	500.56470	500.50012	-.06458	23.2488

Sen-Wyller equations without approximations [*Sen and Wyller*, 1960] was employed to analyze the Faraday rotation data from Nike Apache 14.532. The procedure for analyzing f_F is outlined in Figure 4.8. An initial value for the electron concentration is assumed. From this initial value of electron concentration, the values of the refractive indices for both magnetoionic modes are calculated. The refractive indices are used to obtain a calculated value of f_F corresponding to the initial value of electron concentration. The electron concentration is repeatedly corrected until the calculated value of f_F matches the experimental value. The calculated value of f_F and the experimental value of f_F usually agree to within ± .1% after five or six iterations.

To solve for the electron concentration when only Faraday rotation data are available, a model for the collision frequency must be used (i.e., equation (3.1)). The pressures were taken from the COSPAR International Reference Atmosphere Model [*CIRA*, 1972] and K was equal to 7.5×10^5 $N^{-1}m^2s^{-1}$. The electron concentrations obtained from the analysis of the 3 MHz radio data of Nike Apache 14.532 are given in Table 4.6 and are plotted in Figure 4.9. The error bars correspond to an uncertainty of ± 3 deg s^{-1} in the Faraday rotation rate obtained by applying equation (4.22) to the data between 35 and 52 km under the assumption of free space conditions.

4.4 *Probe Current Calibration*

Variations of electron concentration with altitude are believed to be accurately represented by changes in probe current [*Mechtly et al.*, 1967]. However, exact equations giving electron concentration as a function of probe current, collision frequency, rocket velocity, and other parameters do not exist. For this reason, dc-probe current, I, is calibrated by values of electron concentration, N, from the radio-propagation experiment. The

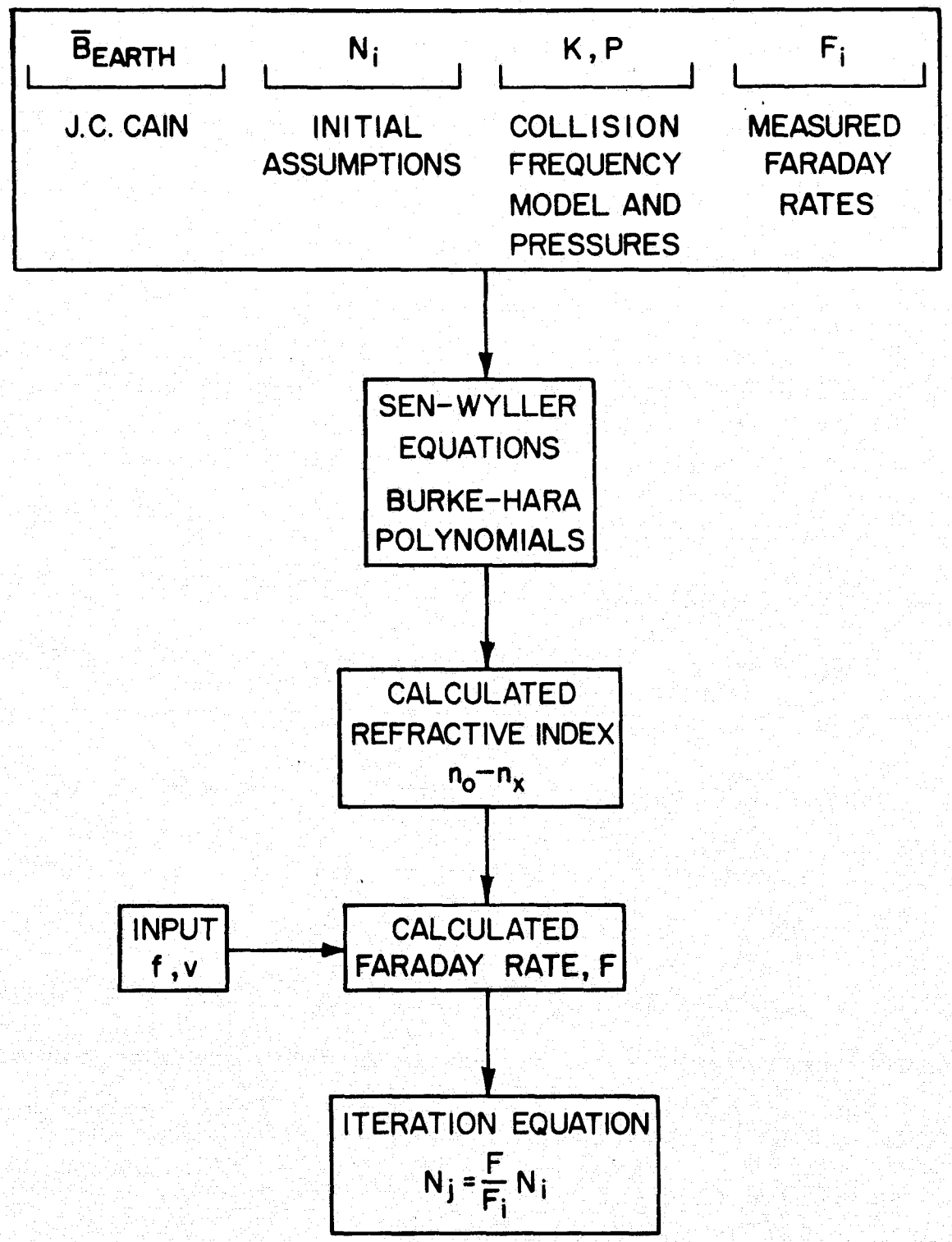

Figure 4.8 Procedure for analyzing Faraday rotation rates.

TABLE 4.6

Electron concentration calculated from 3 MHz radio data of Nike Apache 14.532

Center Time (s)	$N(m^{-3})$
72.0	1.484277×10^{10}
72.5	7.311761×10^{9}
73.0	6.887715×10^{9}
73.5	1.596224×10^{10}
74.0	2.457148×10^{10}
74.5	2.314058×10^{10}
75.0	1.605942×10^{10}

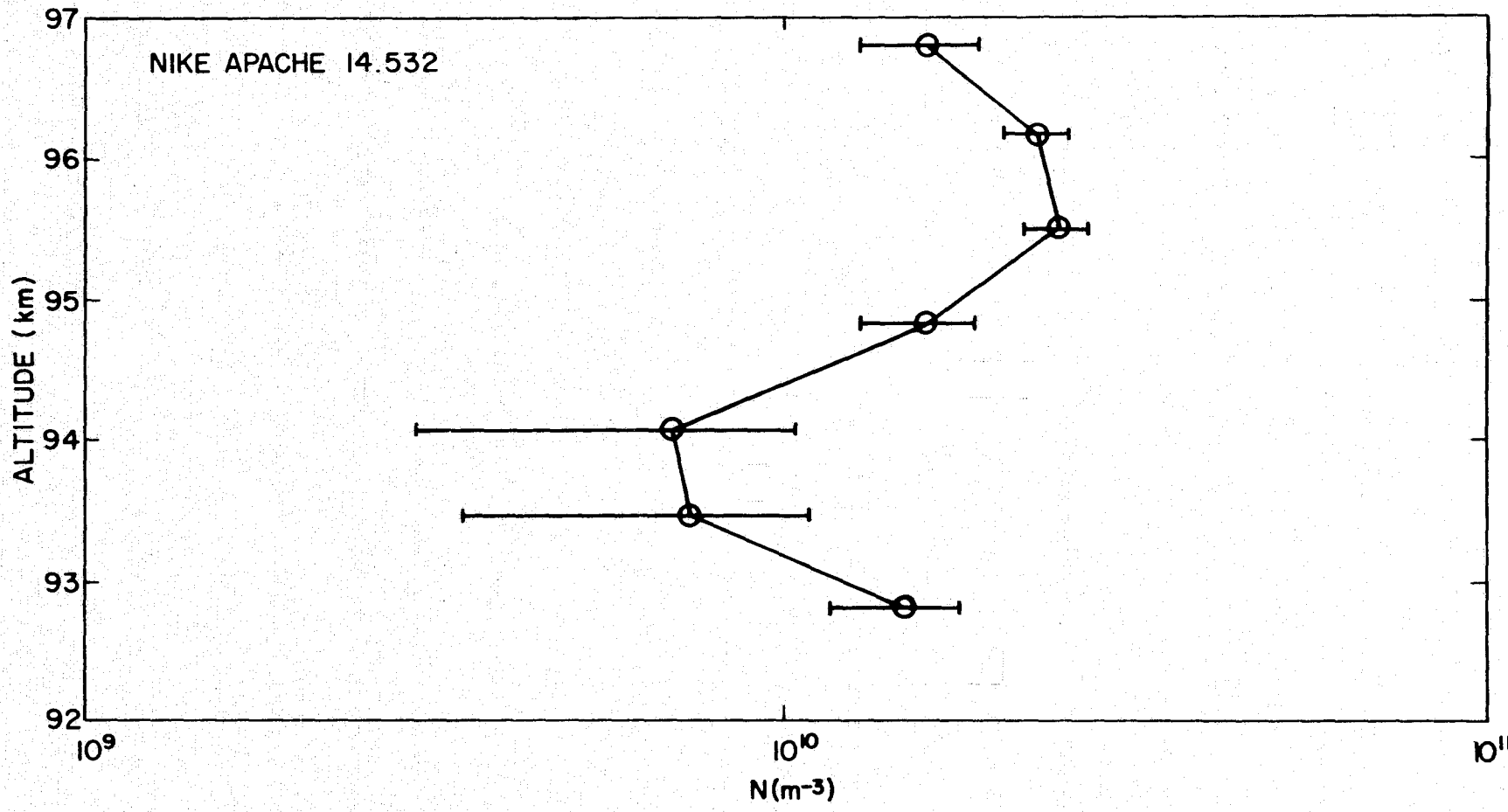

Figure 4.9 Plot of N obtained from the analysis of the Faraday rotation rates from Nike Apache 14.532.

N/I ratio is calculated for each value of N from the radio data analysis and from corresponding weighted mean values of I. The values for N, I, and N/I for Nike Apache 14.532 are tabulated in Table 4.7. These N/I values are plotted as a function of altitude in Figure 4.10.

The altitudes of the 2 MHz and 3 MHz ordinary mode reflection points are derived from the times at which the AGC voltages of the rocket receivers indicated a loss of signal.

The reflection of the 2 MHz ordinary mode occurred at 77.85 S ET which corresponds to an altitude of 100.6 km. The critical value of N is 5.54 x 10^4 cm^{-3} at this point.

The reflection of the 3 MHz ordinary mode occurred at 111.57 S ET which corresponds to an altitude of 139.1 km. The critical value of N is 1.23 x 10^5 cm^{-3} at this point.

Past experience shows that N/I is nearly constant between about 100 and 150 km. Therefore, the calibration between 105 and 120 km is set at the value determined by the 3 MHz ordinary mode reflection point, 5.6 x 10^9 cm^{-3} A^{-1}.

Past experience shows that a transition in N/I occurs at the steep gradient in electron concentration at the mesopause. The point (2.8 x 10^9 cm^{-3} A^{-1}, 86.5 km) corresponds to the intersection of a plateau and a steep gradient of the probe current. Between 86.5 and 105 km, the equation for the straight line passing through the 2-MHz ordinary mode reflection point and the point (2.8 x 10^9 cm^{-3} A^{-1}, 86.5 km) is

$$N/I(z) = 2.8 \times 10^9 \exp\left(\frac{z-86.5}{26.834}\right), \quad 86.5 \leq z \leq 105 \text{ km}. \qquad (4.25)$$

The error bars in this region are extrapolations of the uncertainty of ± 3 deg s^{-1} previously determined for the Faraday rotation rates under the

TABLE 4.7

The N, I and N/I values from Nike Apache 14.532.

Altitude (km)	N (m^{-3})	Weighted I (A)	N/I ($m^{-3}A^{-1}$)
92.795	1.484277×10^{10}	$.1865 \times 10^{-5}$	7.9586×10^{15}
93.473	7.311761×10^{9}	$.2468 \times 10^{-5}$	2.9626×10^{15}
94.149	6.887715×10^{9}	$.3280 \times 10^{-5}$	2.0999×10^{15}
94.822	1.596224×10^{10}	$.4360 \times 10^{-5}$	3.7070×10^{15}
95.493	2.457148×10^{10}	$.5450 \times 10^{-5}$	4.5085×10^{15}
96.162	2.314058×10^{10}	$.6526 \times 10^{-5}$	3.5459×10^{15}
96.828	1.605942×10^{10}	$.7474 \times 10^{-5}$	2.1487×10^{15}

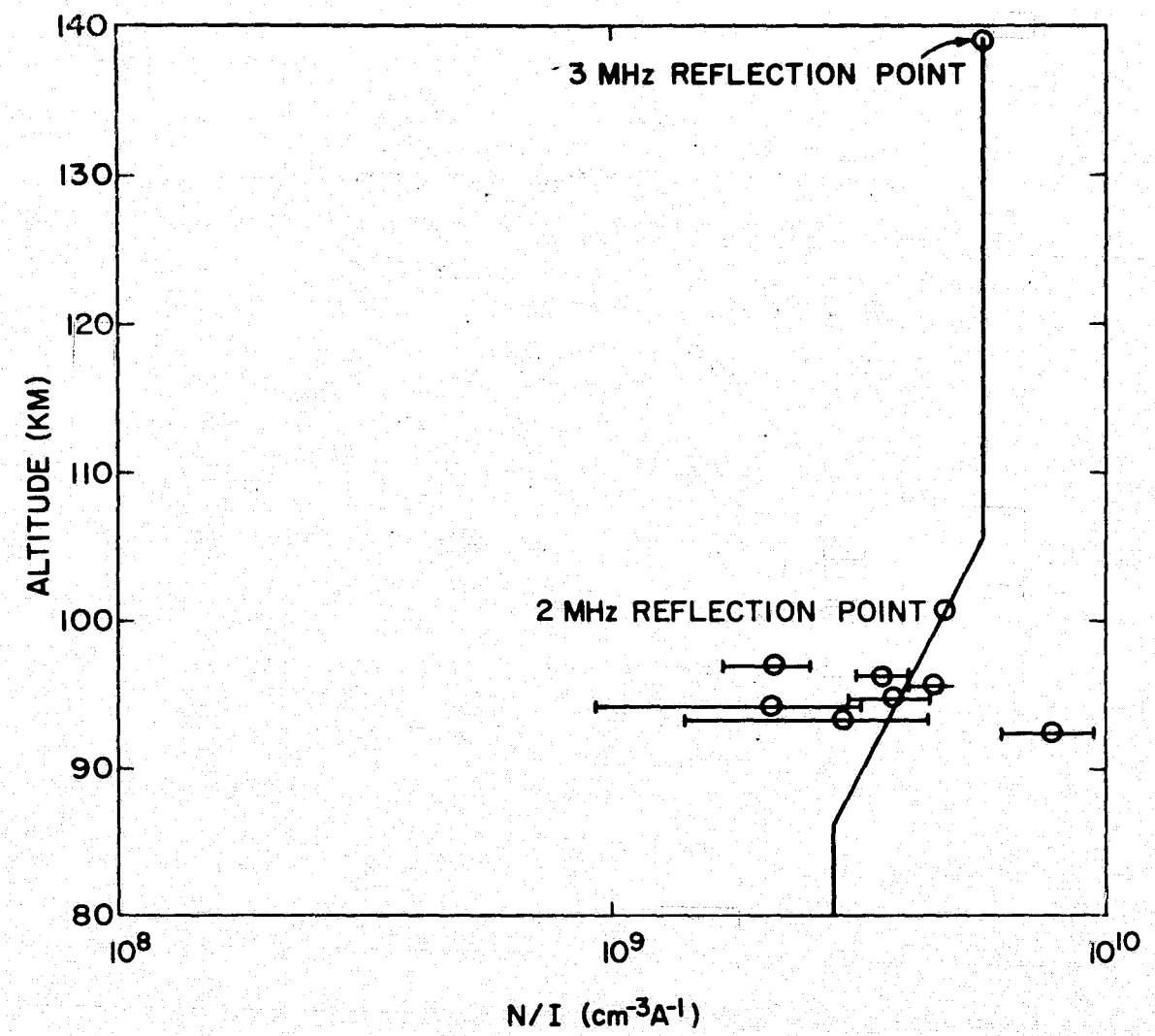

Figure 4.10 *N/I* calibration curve for Nike Apache 14.532.

assumption of free-space conditions between 35 and 52 km.

The constant value 2.8×10^9 cm^{-3} A^{-1} is assumed as the calibration below 86.5 km.

For each second of the flight, ten values of electron probe current are multiplied by the appropriate values of N/I from the smoothed curve of Figure 4.10. Since the present method of data processing is based on sampling of the probe current at equal intervals in time, the points are unevenly spaced in altitude because of the changing velocity of the rocket. K. L. Miller's program [*Edwards*, 1973] was used to interpolate electron concentrations at 0.1 km intervals. The final results are presented in Chapter 5.

5. CONCLUSIONS

The final profile of electron concentration from Nike Apache 14.532 is shown in Figure 5.1. Corresponding numerical values of electron concentration are tabulated in Table 5.1.

The model profile, used to calculate the anticipated differential absorption rates in Section 3.1, is also shown in Figure 5.1.

The profile labeled K14 in Figure 5.1 is a profile obtained by *Kane* [1974] at a solar zenith angle of 14 degrees from rocket measurements of radio-wave absorption conducted from the equatorial site at Thumba, India on March 8, 1968. Both rockets, 14.532 and K14, were launched on one of the five quietest days of their respective months, in terms of magnetic activity and disturbances. Each day was designated "QQ" by World Data Center A for Solar-Terrestrial Physics [*Lincoln*, 1968; 1975].

A comparison of these profiles reveals that:

1. There is good agreement between the model profile and the profile of Nike Apache 14.532. This observation supports the conclusion that for a solar zenith angle of 60°, differential absorption at the geomagnetic equator is too small to measure by present techniques. (cf. Section 3.1).
2. All three profiles exhibit a plateau of electron concentration. The plateau in electron concentration occurs at a higher altitude in the model and 14.532 profiles than in K14.
3. The electron concentrations measured by Kane are larger by a factor of approximately 4.
4. A steep gradient in electron concentration, beginning at 86.5 km, is evident in the profile of 14.532.
5. The ratio $N_m D(\text{K14})/N_m D(14.532) = 3.4$, where $N_m D$ is the value of

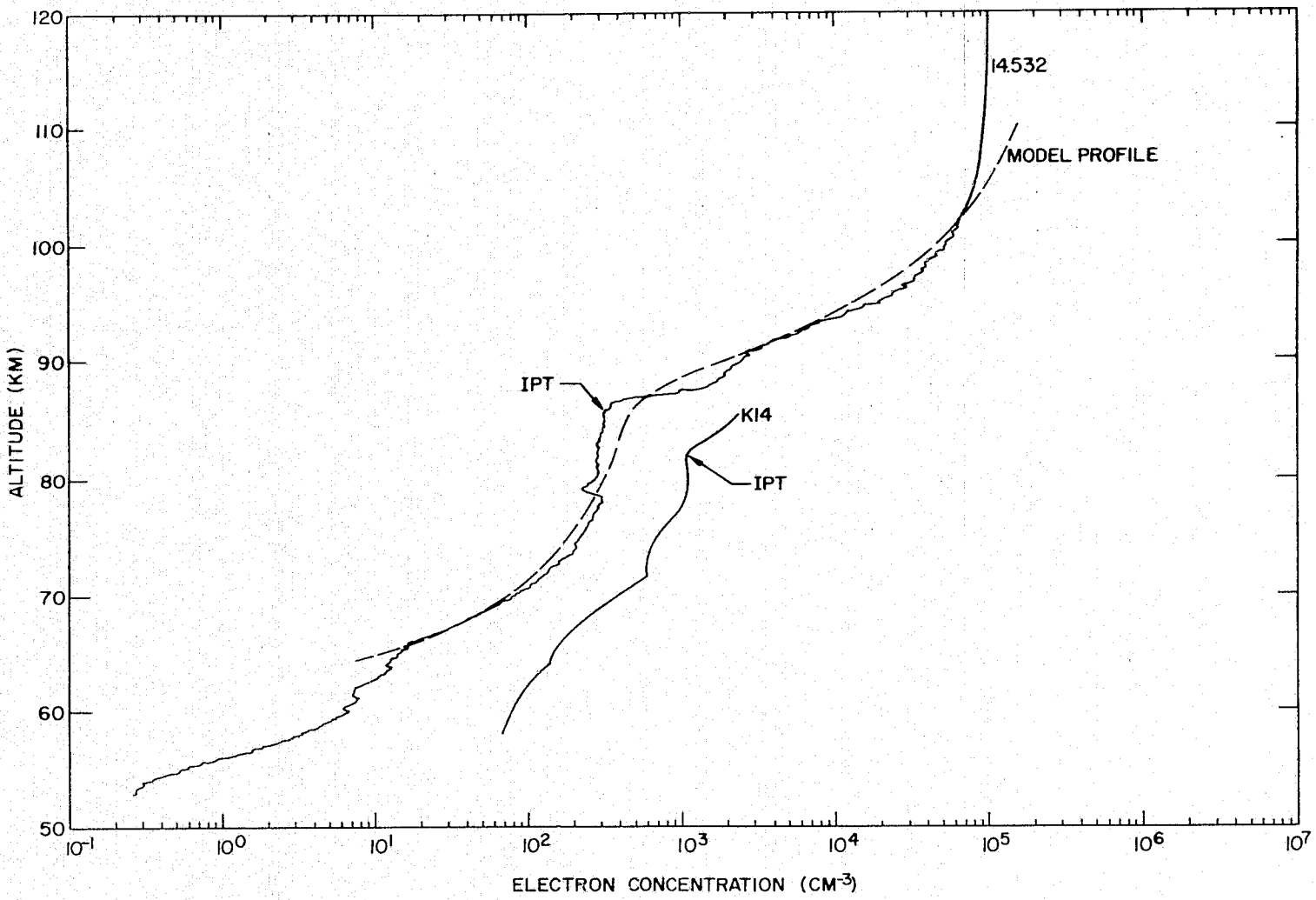

Figure 5.1 Profiles of electron concentration. The inflection points, denoted IPT, for 14.532 and K14 are (3.23×10^{2} cm^{-3}, 86 km) and (1.10×10^{3} cm^{-3}, 82.7 km), respectively.

Table 5.1

Electron concentration table: Nike Apache 14.532 launched 28 May 1975 at 20:26:00 UT
Punta Chilca, Peru (12.6 S lat, 76.8 W long) CHI=60 deg, electron concentration (M-3).

ALTITUDE (KM)	+.0	+.1	+.2	+.3	+.4	+.5	+.6	+.7	+.8	+.9
52								2.55E 05	2.56E 05	2.65E 05
53	2.67E 05	2.68E 05	2.69E 05	2.74E 05	2.82E 05	2.87E 05	2.93E 05	3.04E 05	3.03E 05	2.94E 05
54	3.23E 05	3.43E 05	3.47E 05	3.65E 05	3.85E 05	3.97E 05	4.22E 05	4.57E 05	4.58E 05	5.24E 05
55	5.15E 05	5.57E 05	6.01E 05	5.86E 05	6.26E 05	7.17E 05	7.26E 05	7.57E 05	8.48E 05	8.92E 05
56	9.23E 05	9.86E 05	1.09E 06	1.22E 06	1.24E 06	1.32E 06	1.54E 06	1.56E 06	1.55E 06	1.73E 06
57	1.82E 06	1.85E 06	2.02E 06	2.17E 06	2.27E 06	2.35E 06	2.46E 06	2.72E 06	2.85E 06	2.89E 06
58	3.13E 06	3.20E 06	3.28E 06	3.46E 06	3.65E 06	3.76E 06	3.95E 06	4.18E 06	4.35E 06	4.47E 06
59	4.54E 06	4.85E 06	5.06E 06	5.18E 06	5.33L 06	5.59E 06	5.62E 06	5.86E 06	6.14E 06	6.37E 06
60	6.61E 06	6.87E 06	6.52E 06	6.65E 06	6.21E 06	6.40E 06	6.70E 06	7.17E 06	7.46E 06	7.63E 06
61	7.61E 06	7.66E 06	7.68E 06	7.35E 06	7.08E 06	7.13E 06	7.18E 06	7.22E 06	7.27E 06	7.31E 06
62	7.36E 06	7.41E 06	7.63E 06	7.59E 06	6.36E 06	6.73E 06	9.10E 06	9.46E 06	9.83E 06	1.02E 07
63	1.04E 07	1.07E 07	1.11E 07	1.14E 07	1.18E 07	1.19E 07	1.21E 07	1.26E 07	1.29E 07	1.26E 07
64	1.17E 07	1.18L 07	1.20E 07	1.22E 07	1.24E 07	1.25E 07	1.29E 07	1.31E 07	1.35E 07	1.38E 07
65	1.39E 07	1.41C 07	1.50E 07	1.52C 07	1.49E 07	1.56E 07	1.61E 07	1.65E 07	1.61E 07	1.60E 07
66	1.66E 07	1.71C 07	1.82E 07	2.11F 07	2.20E 07	2.24C 07	2.36E 07	2.47E 07	2.57E 07	2.61E 07
67	2.70E 07	2.84E 07	3.02E 07	3.12E 07	3.17L 07	3.24E 07	3.40E 07	3.65E 07	3.80E 07	3.92E 07
68	4.00E 07	4.08E 07	4.26E 07	4.33L 07	4.63E 07	4.86E 07	5.08E 07	5.27E 07	5.44E 07	5.56E 07
69	5.76E 07	6.04E 07	6.33E 07	6.56E 07	6.71E 07	6.73E 07	7.07E 07	7.50E 07	7.76E 07	7.85E 07
70	7.92E 07	8.21E 07	8.38E 07	8.53E 07	8.94E 07	9.20E 07	9.45E 07	1.01E 08	1.04E 08	1.03E 08
71	1.03E 08	1.07E 08	1.13E 08	1.16E 08	1.17E 08	1.18E 08	1.21E 08	1.24E 08	1.26E 08	1.29E 08
72	1.32E 08	1.36E 08	1.38E 08	1.39E 08	1.40E 08	1.44E 08	1.51E 08	1.55E 08	1.60E 08	1.59E 08
73	1.56E 08	1.63E 08	1.68E 08	1.74E 08	1.78E 08	1.63E 08	1.88E 08	1.95E 08	1.97E 08	1.99E 08
74	2.03E 08	2.06E 08	2.11E 08	2.06E 08	2.01E 08	1.99E 08	2.06E 08	2.11E 08	2.15E 08	2.17E 08
75	2.20E 08	2.24E 08	2.24E 08	2.27E 08	2.30E 08	2.34E 08	2.38E 08	2.41E 08	2.43E 08	2.46E 08
76	2.50E 08	2.54E 08	2.55E 08	2.56E 08	2.56E 08	2.65E 08	2.68E 08	2.69E 08	2.69E 08	2.70E 08
77	2.72E 08	2.76E 08	2.78E 08	2.81E 08	2.89E 08	2.93E 08	2.93E 08	2.86E 08	2.87E 08	2.93E 08
78	3.04E 08	3.07E 08	3.07E 08	3.02E 08	3.08E 08	3.09E 08	3.05E 08	2.86E 08	2.72E 08	2.60E 08
79	2.44E 08	2.33E 08	2.27E 08	2.29E 08	2.39E 08	2.47E 08	2.49E 08	2.54E 08	2.60E 08	2.68E 08
80	2.74E 08	2.72E 08	2.77E 08	2.86E 08	2.90E 08	2.91E 08	2.89E 08	2.92E 08	2.91E 08	2.65E 08
81	2.82E 08	2.81E 08	2.82E 08	2.91E 08	2.90E 08	2.84E 08	2.78E 08	2.81E 08	2.85E 08	2.84E 08
82	2.87E 08	2.89E 08	2.87E 08	2.87E 08	2.88E 08	2.90E 08	2.89E 08	2.94E 08	2.95E 08	2.87E 08
83	2.86E 08	2.87E 08	2.88E 08	2.95E 08	2.93E 08	2.89E 08	2.97E 08	3.02E 08	3.04E 08	3.01E 08
84	3.00E 08	3.03E 08	3.11E 08	3.12E 08	3.09E 08	3.02E 08	3.19E 08	3.17E 08	3.13E 08	3.12E 08
85	3.16E 08	3.19E 08	3.18E 08	3.17E 08	3.16E 08	3.17E 08	3.18E 08	3.12E 08	3.13E 08	3.20E 08
86	3.23E 08	3.36E 08	3.49E 08	3.54E 08	3.47E 08	3.48E 08	3.59E 08	3.84E 08	4.10E 08	4.35E 08
87	4.56E 08	5.06E 08	5.26E 08	6.69E 08	9.15E 08	9.86E 08	1.01E 09	1.03E 09	1.32E 09	1.47E 09
88	1.52E 09	1.54E 09	1.61E 09	1.86E 09	1.74E 09	1.76E 09	1.79E 09	1.85E 09	1.96E 09	1.99E 09
89	1.98E 09	1.94E 09	1.98E 09	2.03E 09	2.08E 09	2.13E 09	2.16E 09	2.19E 09	2.25E 09	2.39E 09
90	2.44L 09	2.49E 09	2.59E 09	2.62E 09	2.66E 09	2.67E 09	2.88E 09	2.73E 09	2.71E 09	2.84E 09
91	3.04E 09	3.25E 09	3.37E 09	3.39E 09	3.49E 09	3.70E 09	3.84E 09	3.74E 09	3.81E 09	4.02E 09
92	4.35E 09	5.00E 09	5.10E 09	5.36E 09	5.82E 09	5.94E 09	6.04E 09	6.21E 09	6.47E 09	6.60E 09
93	6.97E 09	7.13E 09	7.05E 09	7.83E 09	8.13E 09	8.37E 09	9.16E 09	1.00E 10	1.06E 10	1.14E 10
94	1.17E 10	1.19E 10	1.22E 10	1.24E 10	1.25E 10	1.36E 10	1.48E 10	1.56E 10	1.57E 10	1.58E 10
95	1.73E 10	2.03E 10	1.95E 10	2.00E 10	2.08E 10	2.15E 10	2.22E 10	2.36E 10	2.45E 10	2.41E 10
96	2.44E 10	2.58E 10	2.61E 10	2.71E 10	2.91C 10	3.00E 10	2.96E 10	2.79E 10	2.99E 10	3.18E 10
97	3.32E 10	3.37E 10	3.31E 10	3.33E 10	3.36E 10	3.46E 10	3.54E 10	3.74E 10	3.85E 10	3.92E 10
98	3.68E 10	3.75E 10	3.91E 10	4.04F 10	3.97E 10	3.67E 10	3.90E 10	4.06E 10	4.11E 10	4.17E 10
99	4.25E 10	4.4AE 10	4.63F 10	4.60E 10	4.63E 10	4.70E 10	4.76E 10	5.18E 10	5.22E 10	5.18E 10
100	5.31E 10	5.34E 10	5.37E 10	5.29E 10	5.41E 10	5.42E 10	5.65E 10	5.82E 10	5.90E 10	5.97E 10
101	6.07E 10	5.90E 10	5.84E 10	6.15E 10	6.24E 10	6.32E 10	6.39E 10	6.44E 10	6.26E 10	6.43E 10
102	6.52E 10	6.52E 10	6.52E 10	6.53E 10	6.50E 10	6.71E 10	6.98E 10	6.83E 10	6.67E 10	6.50E 10
103	6.45E 10	6.72E 10	6.80E 10	6.84F 10	6.88E 10	6.51E 10	6.54E 10	7.01E 10	7.24E 10	7.51E 10
104	7.51E 10	7.51E 10	7.51E 10	7.61E 10	7.81E 10	7.75E 10	7.68E 10	7.62E 10	7.56E 10	7.52E 10
105	7.80E 10	8.02E 10	8.13E 10	8.16E 10	8.19C 10	8.22E 10	8.25E 10	8.13E 10	7.91E 10	8.02E 10
106	8.13E 10	8.24E 10	8.35E 10	8.47E 10	8.63E 10	8.70E 10	8.76E 10	8.82E 10	8.86E 10	8.93E 10
107	8.75E 10	8.87E 10	8.77E 10	8.75E 10	8.82E 10	8.88E 10	8.94E 10	9.02E 10	9.10E 10	9.19E 10
108	9.26E 10	9.34E 10	9.27E 10	8.93E 10	9.12E 10	9.26E 10	9.40E 10	9.53E 10	9.62E 10	9.27E 10
109	9.27E 10	9.38E 10	9.51E 10	9.64E 10	9.77E 10	9.42E 10	9.05E 10	9.07E 10	9.16E 10	9.25E 10
110	9.33E 10	9.48E 10	9.53E 10	9.27L 10	9.34E 10	9.42E 10	9.50E 10	9.22E 10	8.98E 10	9.27E 10
111	9.23E 10	9.18E 10	9.12E 10	9.00E 10	8.99E 10	9.73E 10	9.61E 10	9.46E 10	9.35E 10	9.21E 10
112	9.14E 10	9.09E 10	9.44E 10	9.43E 10	9.02E 10	8.92E 10	9.15E 10	9.77E 10	9.51E 10	9.35E 10
113	9.37E 10	9.39E 10	9.41L 10	9.66E 10	9.48E 10	9.32E 10	9.27E 10	9.22E 10	9.17E 10	9.66E 10
114	9.53E 10	9.42E 10	9.49E 10	9.56E 10	9.64E 10	9.67E 10	9.45E 10	9.36E 10	9.31E 10	9.26E 10
115	9.22E 10	9.79E 10	9.87E 10	9.77E 10	9.68E 10	9.57E 10	9.48E 10	9.52E 10	9.76E 10	9.60E 10
116	9.51E 10	9.47E 10	9.39E 10	1.00E 11	9.90E 10	9.60E 10	9.52E 10	9.65E 10	9.88E 10	1.02E 11
117	9.77E 10	9.66E 10	9.67E 10	9.62E 10	9.73E 10	1.02E 11	9.80E 10	9.64E 10	9.74E 10	9.90E 10
118	1.01E 11	1.00E 11	9.39E 10	9.78E 10	9.64E 10	9.67E 10	9.90E 10	9.88E 10	9.89E 10	1.02E 11
119	1.02E 11	1.02E 11	1.01E 11	1.00E 11	1.00E 11	1.03E 11	1.03E 11	1.02E 11	1.02E 11	1.03E 11
120	1.05E 11	1.06E 11	1.06E 11							

the maximum ionization in the *D* region, just below the steep gradient.

6. No sporadic-E layers are observed.

A characteristic feature of daytime profiles of *D*-region electron concentration, *N*, is a gradient just above an inflection of *N* at altitudes ranging from about 80 to 86 km [*Mechtly and Bilitza*, 1974]. Mechtly and Bilitza showed that N_mD, the value of *N* at the inflection point, is proportional to the square of the cosine of the solar zenith angle, χ

$$N_mD \propto (\cos \chi)^2 \tag{5.1}$$

when the *D* region is unperturbed.

By equation (5.1), the ratio of N_mD for a solar zenith angle of 14 degrees (i.e., K14) to N_mD for a solar zenith angle of 60 degrees (i.e., 14.532) is:

$$\frac{N_mD(\text{K14})}{N_mD(14.532)} = \frac{(\cos 14°)^2}{(\cos 60°)^2} = 3.8 \tag{5.2}$$

This compares with 3.4 calculated from the values of N_mD shown in Figure 5.1.

Thus, profiles K14 and 14.532 support the conclusion that $N_mD \propto (\cos \chi)^2$ when the *D* region is unperturbed.

REFERENCES

Appleton, E. V. (1932), Wireless studies of the ionosphere, *J. Instn. Elec. Engrs. 71*, 642-650.

Bergland, G. D. (1969), A guided tour of the fast Fourier transform, *IEEE Spectrum 6*, 41-52.

Blackman, R. B. and J. W. Tukey (1958), *The Measurement of Power Spectra*, Dover Publications, Inc., New York.

Brigham, E. O. (1974), *The Fast Fourier Transform*, Prentice-Hall, Inc., Englewood Cliffs, New Jersey.

Budden, K. G. (1961), *Radio Waves in the Ionosphere*, Cambridge Univ. Press, Great Britain.

CIRA (1965), *COSPAR International Reference Atmosphere*, North-Holland Publ. Co., Amsterdam.

CIRA (1972), *COSPAR International Reference Atmosphere*, Akademie-Verlag, Berlin.

Edwards, B. (1973) (Ed), Research in Aeronomy: October 1, 1972-March 31, 1973, *Prog. Rep. 73-1*, Aeron. Lab., Dep. Elec. Eng., Univ. Ill., Urbana-Champaign.

Edwards, B. (1974) (Ed), Research in Aeronomy: October 1, 1973-March 31, 1974, *Prog. Rep. 74-1*, Aeron. Lab., Dep. Elec. Eng., Univ. Ill., Urbana-Champaign.

Edwards, B. (1975) (Ed), Research in Aeronomy: October 1, 1974-March 31, 1975, *Prog. Rep. 75-1*, Aeron. Lab., Dep. Elec. Eng., Univ. Ill., Urbana-Champaign.

Ginther, J. C. and L. G. Smith (1975), Studies of the differential absorption rocket experiment, *Aeron. Rep. No. 64*, Aeron. Lab., Dep. Elec. Eng., Univ. Ill., Urbana-Champaign.

Hartree, D. R. (1931), The propagation of electromagnetic waves in a refracting medium in a magnetic field, *Proc. Cambridge Phil. Soc. 27*, 143-162.

International Mathematical and Statistical Libraries, Inc. (1975), IMSL Library 1, *Document #LIB1-0005*, Edition 5.

Kane, J. A. (1974), Rocket-borne radio measurements of D and lower E region electron density profiles at the magnetic equator, *Ind. J. Radio and Space Phys. 3*, 99-103.

Knoebel, H., D. Skaperdas, J. Gooch, B. Kirkwood, and H. Krone (1965), High resolution radio frequency measurements of Faraday rotation and differential absorption with rocket probes, *Coord. Sci. Lab. Rep. #273*, Univ. Ill., Urbana-Champaign.

Knoebel, H. and D. O. Skaperdas (1966), Rocket measurements of Faraday rotation and differential absorption, *Rev. Sci. Instr. 37*, 1395-1400.

Lincoln, J. V. (1968) (Ed), Geomagnetic and solar data, *J. Geophys. Res. 73*, 5019.

Lincoln, J. V. (1975) (Ed), Geomagnetic and solar data, *J. Geophys. Res. 80*, 4404.

Mechtly, E. A., S. A. Bowhill, L. G. Smith and H. W. Knoebel (1967), Lower ionosphere electron density and collision frequency from rocket measurements of Faraday rotation, differential absorption and probe current, *J. Geophys. Res. 72*, 5239-5245.

Mechtly, E. A., K. Seino and L. G. Smith (1969), Lower ionosphere electron densities measured during the solar eclipse of 12 November 1966, *Radio Sci. 4*, 371-375.

Mechtly, E. A., P. E. Monro, N. Golshan and R. S. Sastry (1975), FORTRAN programs for calculating lower ionosphere electron densities and

collision frequencies from rocket data, *Aeron. Rep. No. 37*, Aeron. Lab., Dep. Elec. Eng., Univ. Ill., Urbana-Champaign.

Mechtly, E. A. (1974), Accuracy of rocket measurements of lower ionosphere electron concentrations, *Radio Sci. 9*, 373-378.

Mechtly, E. A. and D. Bilitza (1974), Models of D-region electron concentration from rocket data, Institut für Physikalische Weltraumforschung Heidenhofstrasse 8, 7800 Freiburg, FRG.

Oppenheim, A. V. and R. W. Schafer (1975), *Digital Signal Processing*, Prentice Hall, Englewood Cliffs, New Jersey.

Phelps, A. V. and J. L. Pack (1959), Electron collision frequencies in nitrogen and in the lower ionosphere, *Phys. Rev. Lett. 3*, 340-342.

Prakash, S., B. H. Subbaraya and S. P. Gupta (1972), Rocket measurements of ionization irregularities in the equatorial ionosphere at Thumba and identificiation of plasma instabilities, *Ind. J. Radio and Space Phys. 1*, 72-80.

Sen. H. K. and A. A. Wyller (1960), On the generalization of the Appleton-Hartree magnetoionic formulas, *J. Geophys. Res. 65*, 3931-3950.

Schutz, S. R., L. G. Smith and H. D. Voss (1975), Electron heating rates in the E and lower F regions, *Radio Sci. 10*, 289-295.

Smith, L. G. (1967), *COSPAR Information Bulletin 17*, (Ed) K. Maeda, revised edition.

APPENDIX I

Computer Program for Determining the Spectra of Finite Length Discrete Time Sequences

```
C       IWK MUST BE FOUND IN CORE ON A BOUNDRY DIVISIBLE BY 8
C       INTEGER*4 IWK(18050) WILL ONLY WORK HALF THE TIME
C       THIS IS BECAUSE IT IS USED AS A STORAGE AREA FOR A REAL
C                                                  *4 VARIABLE IN FFT

        REAL*8 IWK(9025)
        INTEGER*2 ARRAY(32128)
        REAL*8 DATA(6000)
        COMPLEX*16 GAMN
        REAL*4 DMAG(3000),FREQ(200)
        INTEGER*4 DATAID(20)
        EQUIVALENCE(DATA,DMAG)
        NAMELIST/FRAMS/NRGO,NSNGO,NELT,NELN
        ASSIGN 999 TO KILL
        READ(5,979) DATAID
979     FORMAT(5X,20A4//4)
        WRITE(6,578) DATAID
978     FORMAT(5X,20A4//)
        CALL TPOPIZ(12)
C       NRGO IS FIRST RECORD NUMBER
C       NSNGO IS FIRST SCAN NUMBER IN RECORD
C       NELT IS ELEMENT NUMBER IN SCAN
C       NELN IS NUMBER OF ELEMENTS TO BE USTD.
C       WARNING - USER MUST  COMPUTEALL OF THESE VALUES CAREFULLY
C       PLOTTING SEQUENCE **********************
        NCRV=30
C       GENERATE FREQ. ARRAY (MINUS TO MOVE DOWN THE PAGE)
        DIMENSION SCA(2),SCF(2)
        DO 8 NF=1,180
8       FREQ(NF)=1-NF
C       FIRST DRAW FREQ. CCALE
C       ,TART AT ZERO, THEN GO AT 20. PER INCH(FOR 8 INCH AXIS)
        SCF(1)=0.0
        SCF(2)=20.
        CALL PLOT(.5,.5,-3)
        CALL CCP5AX(0.,9.,'LOW FREQ (HZ)',-13,3.,-90.,SCF)
        SCF(1)=440.
        CALL CCP5AX(0.,6.,'FREQUENCY (HZ)',-14,6.,-90.,SCF)
C       READY SCALE FACTOR FOR FREQ ARRAY
        SCF(1)= -180.0
C       SET UP TIME AXIS.(NCRV = # OF PLOTS TO MAKE)
        SCA(1)= 1.
        SCA(2)=1.
        DIST = NCRV
        CALL CCP5AX(0.,0.,'TIME(RELATIVE)',-14,DIST,0.,SCA)
        CALL CCP5AX(0.,9.,'TIME(RELATIVE)', 14,DIST,0.,SCA)
C       PLOTTING SEQUENCE **********************
43      CONTINUE
        READ (5,FRAMS)
        WRITE(6,889)NRGO,NSNGO,NELT,NELN
```

```
889   FORMAT(1X,9I10)
C     FORMAT DATA CARD &PRAMS NRGO=4000,NSNGO=20,   ETC    ,&END
      IF(NRGO.EQ.0) GO TO 42
C     TAPE HANDLING ROUTINES
      IF(NRGO.EQ.1) CALL TPBSRZ(12)
      IF(NRGO.EQ.0) GO TO 42
      IF(NRGO.EQ.1) GO TO 41
      KSKIP = NRGO -1
      DO 40 N=1,KSKIP
      CALL TPFSRZ(12)
40    CONTINUE
41    FNTOP=FLOAT(NELN+NSNGO)/400.
      NTOP=IFIX(FNTOP)+1
      KNSNGO=IFIX(400.*(FNTOP+FLOAT(1-NTOP)))
      DO 50 N=1,NTOP
      M=(N-1)*2008 + 1
      CALL TPGETZ(12,ARRAY(M))
      CALL TPCHKZ(12,NTAPE,KILL)
      IGO=M+1999
      ISTOP = IGO+ 8
      WRITE(6,104)(ARRAY(I),I=IGO,ISTOP)
104   FORMAT(1X,9Z10)
C     NTAPE = # OF BYTES TRANSFERRED
50    CONTINUE
      WRITE(6,102) ARRAY(2006),ARRAY(2007),ARRAY(2008),NTAPE
102   FORMAT(1H0,'   TIME CODE   ',4Z10)
42    N005=2005
      NA=NSNGO*5+NELT
      DO 10 N=1,NELN
      DATA(N)= ARRAY(NA)
      NA=NA+5
      IF(NA.LE. N005 ) GO TO 10
      NA=NA+8
      N005 = N005+2008
10    CONTINUE
C     AT THIS POINT, "DATA" IS READY FOR WINDOWING
      NELN2=NELN/2
      FLN2=NELN2
      STT=1.+1./FLOAT(NELN)
      GBASE = 0.01111
      DO 20 K=1,NELN2
      DEL = 3.0*(STT-FLOAT(K)/FLN2)
      G=EXP(-0.5*DEL*DEL)-GBASE
      DATA(K) = G*DATA(K)
      KTP=NELN-K+1
      DATA(KTP) = G*DATA(KTP)
20    CONTINUE
C     NOT NEEDED NOW ------ REMOVE CODE COMPLETELY LATER
      IF(NCRV.NE.0) GO TO 7
      IGO=NELN2 - 100
      ISTOP = IGO + 199
      WRITE(6,105)(DATA(I),I=IGO,ISTOP)
105   FORMAT(10(1X,E9.2))
7     CONTINUE
```

```
C       **********
        CALL FFTR(DATA,GAMN,NELN,IWK)
C       AT THIS POINT, "DATA " CONTAINS THE COMPLEX SPECTRUM.
C       WRITE IT OUT
C       CONVERT TO MAGNUTUDES.    **************
        DO 30 N=1,NELN2
        NT = N*2
        DMAG(N)=DSQRT(DATA(NT)*DATA(NT)+DATA(NT-1)*DATA(NT-1) )
30      CONTINUE
C       WRITE IT OUT IN SELECTED GROUPS    **********
        DO 31 N=1,40,10
        NFREQ = N-1
        NTP = N + 9
31      WRITE(6,103) NFREQ,(DMAG(K),K=N,NTP)
103     FORMAT(1X,I9,10(1X,E9.2))
        DO 32 N = 451,551,10
        NFREQ= N-1
        NTP = N + 9
32      WRITE(6,103) NFREQ,(DMAG(K),K=N,NTP)
C
C******FIND FREQUENCY OF PEAK******
        K1=6
        K2=16
        MAX=5
53      AMAX=0.
        DO 52  K=K1,K2
        IF(DMAG(K).LT.AMAX) GO TO 52
        MAX=K
        AMAX=DMAG(K)
52      CONTINUE
CCCCCC COMPUTE FREQ OF SIG.  ALGORTHIM  <<<<
        MAXM=MAX-1
        MAXP=MAX+1
        RR=ALOG(AMAX/DMAG(MAXP))/ALOG(AMAX/DMAG(MAXM))
        FMAX1=MAX-1
        FSIG=FMAX+.5*(1.0-RR)/1.0+RR)
        WRITE(6,106)FSIG
106     FORMAT(/,' FREQ. OF PEAK = ',F10.5)
        K1=480
        K2=540
        XKM1=DMAG(476)
        XKM=DMAG(477)
        XK=DMAG(478)
        XKP=DMAG(479)
        DO 54 K=K1,K2
        IF(XK.GT.XKM.AND.XKM.GT.XKM1.AND.XK.GT.XKP) GO TO 55
56      XKM1=XKM
        XKM=XK
        XK=XKP
        XKP=DMAG(K)
        GO TO 54
55      MAXM=K-3
        RR=ALOG(XK/XKP)/ALOG(XK/XKM)
        FSIG=MAXM+.5*(1.0-RR)/(1.0+RR)
```

```
      WRITE(6,106) FSIG
      GO TO 56
54    CONTINUE
CCCCCC DANGER<<<< DATA CAN(!) GIVE DIVIDE BY 0
C END OF FREQ. COMPUTATION ON SPECTRAL PEAKS
C
C     PLOTTING SEQUENCE **********************
C     SET UP SCALING FOR ALL PLOTS
      SCA(1)=1.
      IF(NELT.EQ.5) SCA(1)=0.0
      SCA(2)=2.
      CALL XLOGZ(DMAG ,FREQ,60,1,SCA,SCF)
      WRITE(6,101) SCA(1),SCA(2)
101   FORMAT(1X,2E15.5)
      CALL XLOGZ(DMAG(441),FREQ(60),120,1,SCA,SCF)
      CALL PLOT(1.,0.,-3)
C     READY FOR NEXT XLOGZ CALL.
C     PLOTTING SEQUENCE **********************
C     READ NEXT DATA CARD....IF SCAN # = - Z , DO OTHER NELT
C                           ...IF SCAN#=0, READ NEXT NELN ELEMENTS.
      GO TO 43
999   WRITE (6,998) NTAPE
998   FORMAT('   TAPE ERROR   ',I10)
      STOP
      END
```

APPENDIX II

Nike Apache 14.532 Post-Flight Data Tapes

Tape #3, Receiver #1

File 1	Probe Log
File 2	Extraordinary Power #1
File 3	Extraordinary Power #2
File 4	Ordinary Power #1
File 5	Ordinary Power #2

Tape #4, Receiver #1

File 1	Receiver Modulation #1
File 2	500 Hz Reference #1
File 3	Receiver Modulation #2
File 4	500 Hz Reference #2
File 5	Magnetometer

Tape #11, Receiver #3

File 1	Probe Log
File 2	Probe Fine Structure
File 3	Receiver AGC #1
File 4	Receiver AGC #2

Tape #12, Receiver #1

File 1	RF Probe Signal
File 2	Boom Probe Log
File 3	Boom Probe Linear
File 4	RF Probe Monitor
File 5	Magnetometer